and degeneration of elastic fibers also have an important role in wrinkle formation and decreased skin elasticity (Imokawa, 2009). To this extent, the topical application of elastase inhibitors significantly suppressed UV-induced wrinkle formation in hairless mice (Tsuji *et al.*, 2001; Tsukahara *et al.*, 2001; Zhao *et al.*, 2009).

Induction of the expression of heat shock proteins (HSPs), especially that of HSP70, provides resistance to stressors (Morimoto and Santoro, 1998). In addition to this cytoprotective effect, HSP70 has an anti-inflammatory activity (Krappmann *et al.*, 2004; Chen *et al.*, 2006; Tang *et al.*, 2007; Weiss *et al.*, 2007). The artificial expression of HSP70 in keratinocytes and melanocytes confers protection *in vitro* against UV (Maytin *et al.*, 1994; Trautinger *et al.*, 1995; Park *et al.*, 2000; Wilson *et al.*, 2000; Trautinger, 2001). However, the role of HSP70 in photoaging *in vivo* remains unclear. We recently showed that UV-induced skin damage and the resulting inflammatory responses were suppressed in transgenic mice expressing HSP70 (Matsuda *et al.*, 2010). We also reported that UV-induced melanin production by the skin was suppressed in transgenic mice expressing HSP70 (Hoshino *et al.*, 2010). However, the role of HSP70 in UV-induced wrinkle formation is yet to be elucidated.

In this study, we examine the effect of the expression of HSP70 on UV-induced wrinkle formation and decreased skin elasticity. UV-induced epidermal hyperplasia, decreased skin elasticity, and wrinkle formation were suppressed in hairless mice concomitantly subjected to mild heat treatment (exposure to heated water at 42 °C). Moreover, UV-induced epidermal hyperplasia, decreased skin elasticity, the disruption of collagen and elastic fibers, and the basal membrane of the epidermis, and activation of MMPs and elastase were significantly suppressed in transgenic mice expressing HSP70 compared with wild-type mice. These results suggest that HSP70 expression protects the skin against UV-induced wrinkle formation.

RESULTS

Effect of heat treatment on UVB-induced wrinkle formation

We examined the effect of a single mild heat treatment (exposure to heated water, 42 °C for 5 minutes) on HSP expression in the dorsal skin of hairless mice. Immunoblotting analysis revealed that the level of HSP70 but not of other HSPs in the skin increased after the heat treatment (Figure 1a and b). The induction of expression of HSP70 by the mild heat treatment (42 °C for 5 minutes) was observed even after the repeated heat treatment (three times a week for 5 weeks) (Figure 1c and d). Costaining of HSP70 and pan-cytokeratin (a keratinocyte marker), vimentin (a fibroblast marker), or CD11b (a macrophage marker) was observed in both repeatedly heat-treated and untreated dorsal skin (Figure 1e–g). We confirmed mild heat treatment–induced expression of HSP70 in mice irradiated with UVB (Figure 1c–g).

To examine the effect of expression of HSPs on UVB-induced wrinkle formation, the dorsal skin of animals was pre-exposed to the heat treatment (exposure to heated water, 42 °C for 5 minutes) and then irradiated with UVB. This cycle was repeated three times a week for 10 weeks. As shown in Figure 2a and b, visible signs of wrinkling were observed in the dorsal skin of UVB-treated control mice (without heat treatment), but not so clearly in that of mice treated with both UVB and heat. The area of shadow on the replica images, which is indicative of wrinkle formation level, was increased by exposure to UVB radiation, whereas concomitant heat treatment reduced this index in UVB-treated mice (Figure 2c and d). These results suggest that the heat treatment suppresses UVB-induced wrinkle formation.

We then used a Cutometer to examine the effect of heat treatment on UVB-induced alterations to skin elasticity. All indexes of skin elasticity (Uf, final distension; Ue, immediate distension; and Ur, immediate retraction) except for Uv (delayed distension) were decreased by the UVB radiation and were significantly higher in heat-treated skin than in untreated skin exposed to UVB radiation (Figure 2e), suggesting that heat treatment suppresses the UVB-induced decrease in skin elasticity.

Epidermal hyperplasia is also closely linked to wrinkle formation. The UVB irradiation induced epidermal hyperplasia, although the epidermal thickness was lower in mice subjected to concomitant heat treatment than in control mice exposed to UVB radiation (Figure 2f and g).

We then used immunohistochemical analysis to examine the effect of the heat treatment on the ECM. As shown in Figure 3a, the layer expressing type IV collagen (the epidermal basal membrane) was disrupted in UVB-treated control mice (without heat treatment). This effect, however, was attenuated in mice concomitantly exposed to heat treatment.

Total expression of type I collagen and fine collagen fibers was decreased in UVB-exposed control mice (without heat treatment), and these decreases were suppressed in mice that had been concomitantly exposed to heat treatment (Figure 3a). Similar results were observed for elastic fibers, which were identified by the immunohistochemical detection of tropoelastin (Figure 3a). The results in Figure 3a suggest that heat treatment suppressed the UVB-induced disruption and degeneration of the skin's ECM.

UVB-induced wrinkle formation–related phenomena in transgenic mice expressing HSP70

We then compared the UVB-induced decrease in skin elasticity and epidermal hyperplasia between transgenic mice expressing HSP70 (Plumier *et al.*, 1995) and wild-type mice. UVB-induced decreased skin elasticity (decrease in Uf, Ue, and Ur indexes) was observed in wild-type mice; these indexes were significantly higher in UVB-treated transgenic mice expressing HSP70 (Figure 4a). Similar results were observed for epidermal hyperplasia; the epidermal thickness was lower in transgenic mice than in wild-type mice after UVB irradiation (Figure 4b and c). These results show that the UVB-induced decrease in skin elasticity and epidermal hyperplasia observed in wild-type mice was suppressed in transgenic mice expressing HSP70.

The UVB-induced degradation of the epidermal basal membrane and the decrease in collagen and elastic fibers were not observed as clearly in transgenic mice expressing HSP70 as they were in wild-type mice (Figure 3b).

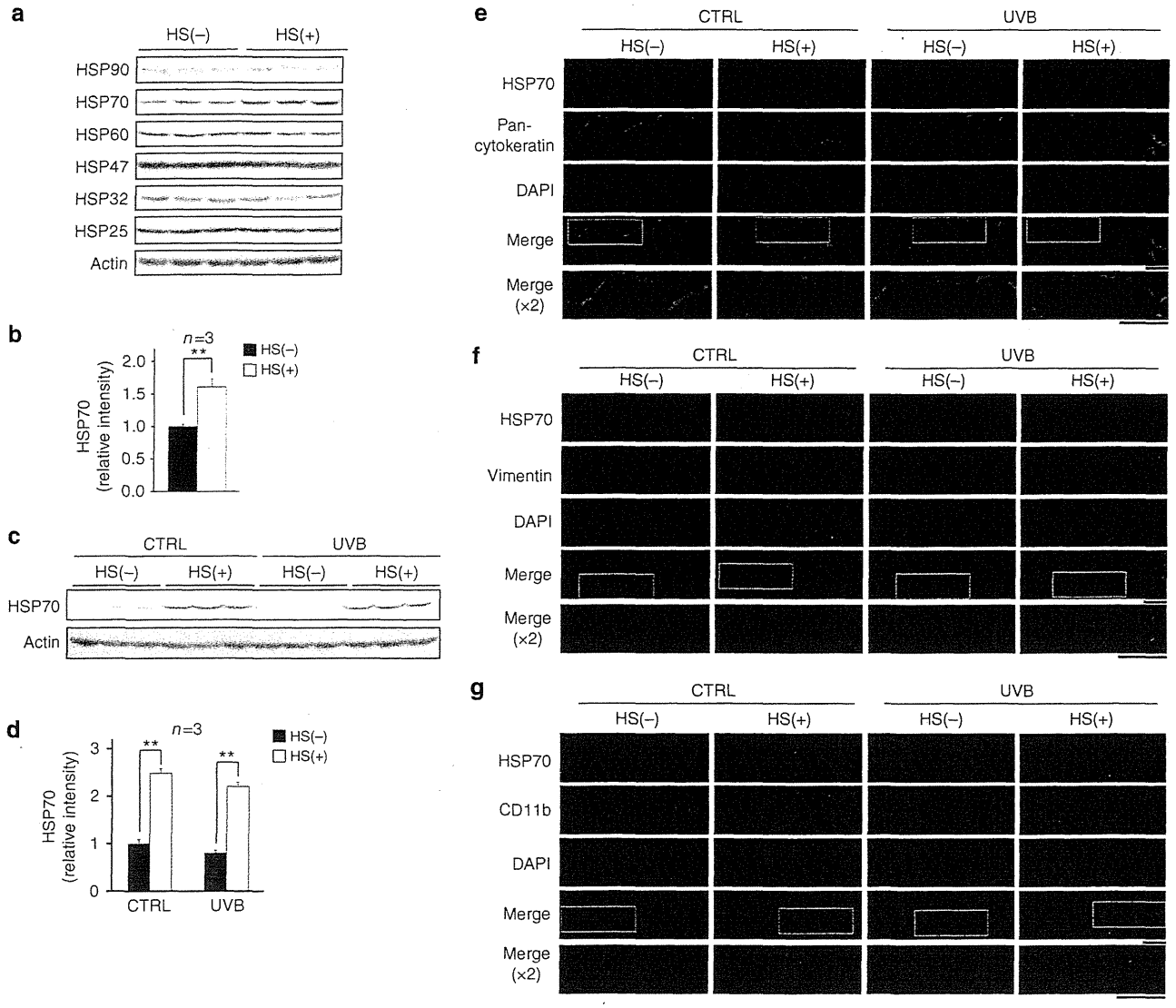

Figure 1. Expression of heat shock proteins (HSPs) in the dorsal skin after heat treatment. (**a**, **b**) The dorsal skin of hairless mice was exposed to heated water at 42 °C (HS(+)) or 37 °C (HS(−)) for 5 minutes. (**c**–**g**) Six hours after this heat treatment, mice were irradiated with UVB. This cycle was repeated three times a week for 5 weeks. (**a**–**g**) Dorsal skin was removed 6 hours after the final heat treatment. (**a**, **c**) Samples were analyzed by immunoblotting with antibodies against each protein. (**b**, **d**) The band intensity was determined. Values are mean ± SEM. $^{**}P<0.01$. (**e**–**g**) Sections were subjected to immunohistochemical analysis with antibodies against HSP70 and pan-cytokeratin (**e**), vimentin (**f**), or CD11b (**g**). Bar = 50 μm. CTRL, control; DAPI, 4,6-diamidino-2-phenylindole dihydrochloride.

Mechanism for the protective role of HSP70 against UVB-induced wrinkle formation–related phenomena

We then determined by TUNEL assay the extent of UVB-induced fibroblast cell death. An increase in the number of TUNEL-positive cells in the skin of wild-type mice was observed after a single UVB irradiation, and this increase was clearly suppressed in transgenic mice expressing HSP70 (Figure 5a). Immunostaining for vimentin was also performed, and the number of cells positive for both TUNEL and vimentin staining was counted. The number of double-positive cells increased in response to UVB irradiation in wild-type mice, and this number was lower in transgenic mice expressing HSP70 (Figure 5b), suggesting that HSP70 expression protected skin fibroblasts from UVB-induced cell death.

To test this idea *in vitro*, we prepared primary cultures of skin fibroblasts from the transgenic and wild-type mice and examined the level of resistance of these cells to hydrogen peroxide. As shown in Figure 5c, treatment of wild-type skin fibroblasts with hydrogen peroxide decreased cell viability; this decrease was significantly suppressed in HSP70-over-expressing skin fibroblasts, showing that the expression of HSP70 protected the skin fibroblasts against reactive oxygen species-induced cell death.

Next, we examined the mechanism for the protective effect of HSP70 against UVB-induced alterations to the ECM. As messenger RNA expression levels corresponding to proα1(I)-collagen, proα2(I)collagen, proα1(IV)collagen, proα2(IV)collagen, and tropoelastin were indistinguishable between transgenic

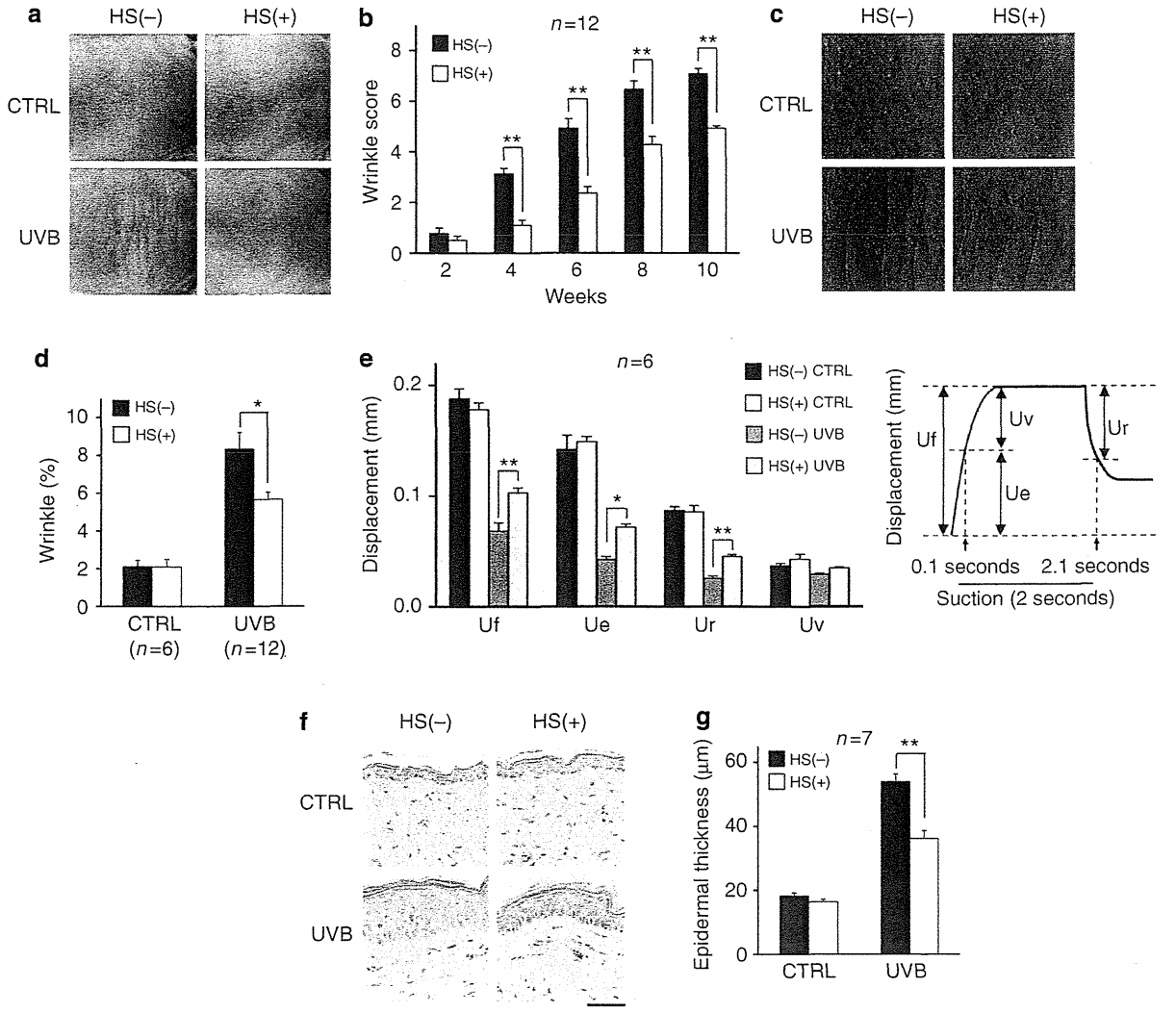

Figure 2. Effect of heat treatment on UVB-induced wrinkle formation. Heat treatment of the dorsal skin was performed, and 6 hours later mice were irradiated with UVB. This cycle was repeated three times a week for 10 weeks. (**a**) Typical photographs of the dorsal skin. (**b**) The wrinkle score was determined. (**c**) Typical replica images of the skin are shown. (**d**) The relative area of wrinkles was calculated. (**e**) Skin elasticity was measured by a Cutometer. The standard time-course profile was shown. (**f–g**) The dorsal skin was removed 24 hours after the final UVB irradiation and sections were subjected to histological examination (**f**). The epidermal thickness was measured (**g**). Values are mean ± SEM. $^{**}P<0.01$; $^{*}P<0.05$. CTRL, control.

mice expressing HSP70 and wild-type mice under conditions both with and without UVB irradiation (data not shown), we then focused on MMPs and elastase. We used gelatin zymography to examine the activities of MMP-2 and MMP-9. The band intensities of MMP-2 and MMP-9, indicative of MMP-2 and MMP-9 activities, were higher in skin tissues prepared from UVB-treated wild-type mice than in those from UVB-treated transgenic mice expressing HSP70 (Figure 6a and b). Similar results were obtained for elastase activity (Figure 6c). On the other hand, the type I collagenase or MMP-13 activity was indistinguishable between the transgenic mice and wild-type mice (Figure 6d and e). The amount of MMP-13 or TIMP-1 in dorsal skin extract was also indistinguishable between them (data not shown). These results suggest that the expression of HSP70 suppresses the UVB-induced activation of MMP-2, MMP-9, and elastase.

To test this idea *in vitro*, we compared the activities of these proteases in primary cultures of skin fibroblasts. The MMP-2 activity was higher in wild-type fibroblasts than in HSP70-expressing fibroblasts in both the presence and absence of hydrogen peroxide (Figure 6f and g). We could not detect MMP-9 activity (Figure 6f). The messenger RNA expression level corresponding to MMP-2 was higher in wild-type fibroblasts than in HSP70-expressing cells (Figure 6h). As for elastase, although the activity in the absence of hydrogen peroxide was indistinguishable between wild-type and HSP70-expressing fibroblasts, the activity was higher in wild-type fibroblasts than in HSP70-expressing fibroblasts in the presence of hydrogen peroxide (Figure 6i). We could not detect messenger RNA expression corresponding to elastase under the conditions used (data not shown). These results support the idea that the expression of HSP70 suppresses MMP-2 and elastase activities.

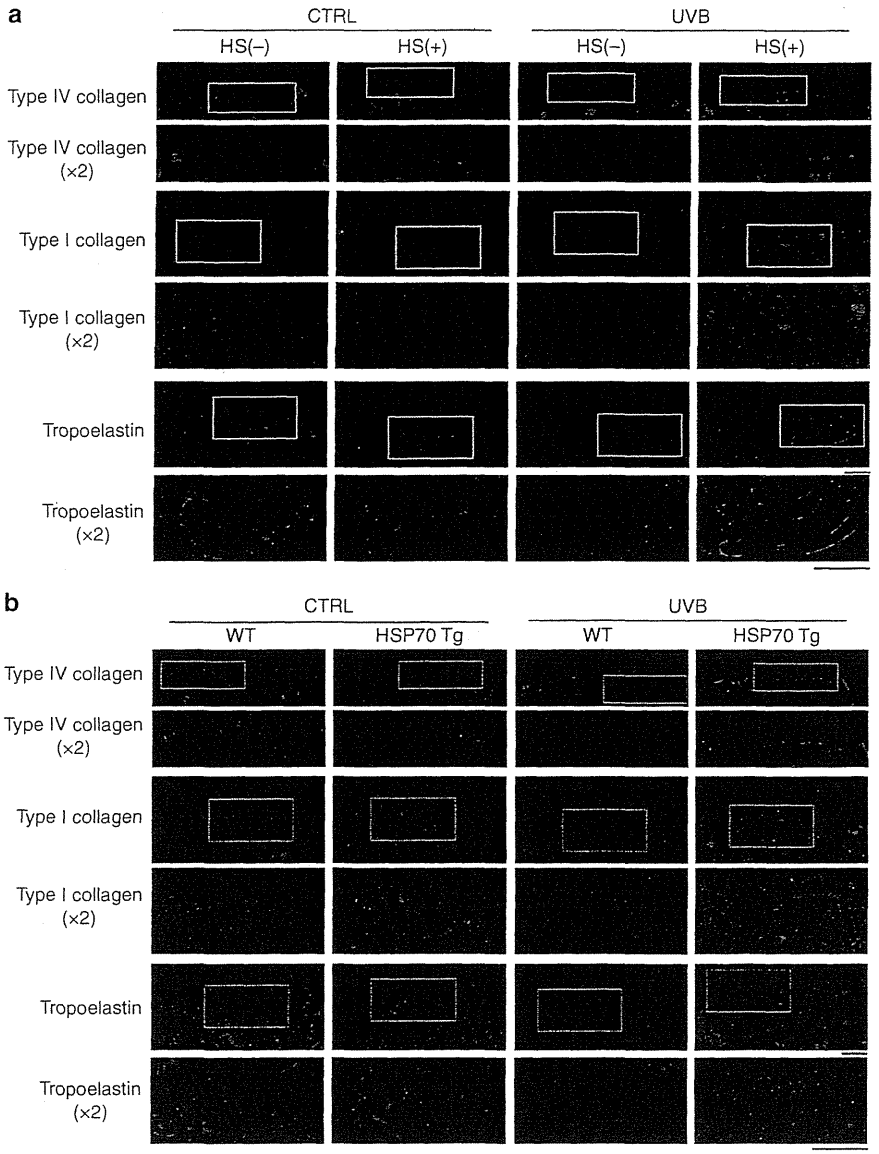

Figure 3. Effect of heat shock protein 70 (HSP70) expression on UVB-induced alteration of extracellular matrix. (**a**) Heat treatment and UVB irradiation of the dorsal skin of hairless mice were performed as described in the legends of Figure 2. (**b**) Transgenic mice expressing HSP70 (HSP70 Tg) and wild-type mice (WT) were irradiated with UVB three times a week for 6 weeks. (**a**, **b**) The dorsal skin was removed 24 hours after the final UVB irradiation and subjected to immunohistochemical analysis with antibodies against type IV collagen, type I collagen, or tropoelastin. Bar = 50 μm. CTRL, control.

In relation to MMP-9, it was reported that inflammatory cells such as macrophages and neutrophils produce this protein (Kessenbrock *et al.*, 2010). We therefore used immunohistochemical analysis to examine the infiltration of these cells in the skin of UVB-treated or untreated transgenic mice expressing HSP70 or their wild-type counterparts. As shown in Figure 6j, the number of CD11b-positive cells (macrophages) or myeloperoxidase-positive cells (neutrophils) in the skin was increased by UVB irradiation in wild-type mice. This number was lower in UVB-treated transgenic mice expressing HSP70, suggesting that the expression of HSP70 inhibits the UVB-induced infiltration of macrophages and neutrophils into the skin. We also used gelatin zymography to compare the activities of MMPs in HSP70-overexpressing and wild-type macrophages, and found that the MMP-9 activity was similar between the two types of macrophages (data not shown). These results suggest that the expression of HSP70 suppresses MMP-9 activity by inhibiting the UVB-induced infiltration of macrophages and neutrophils into the skin.

DISCUSSION

Here we provide data suggesting that HSP70 is protective against UVB-induced wrinkle formation.

UVB-induced wrinkle formation requires a long period of irradiation (about 10 weeks). Thus, it is difficult to monitor UVB-induced wrinkle formation in normal mice (with hair) because a true hairless state with shaved skin can only be maintained for about 6–7 weeks. For this reason, hairless mice

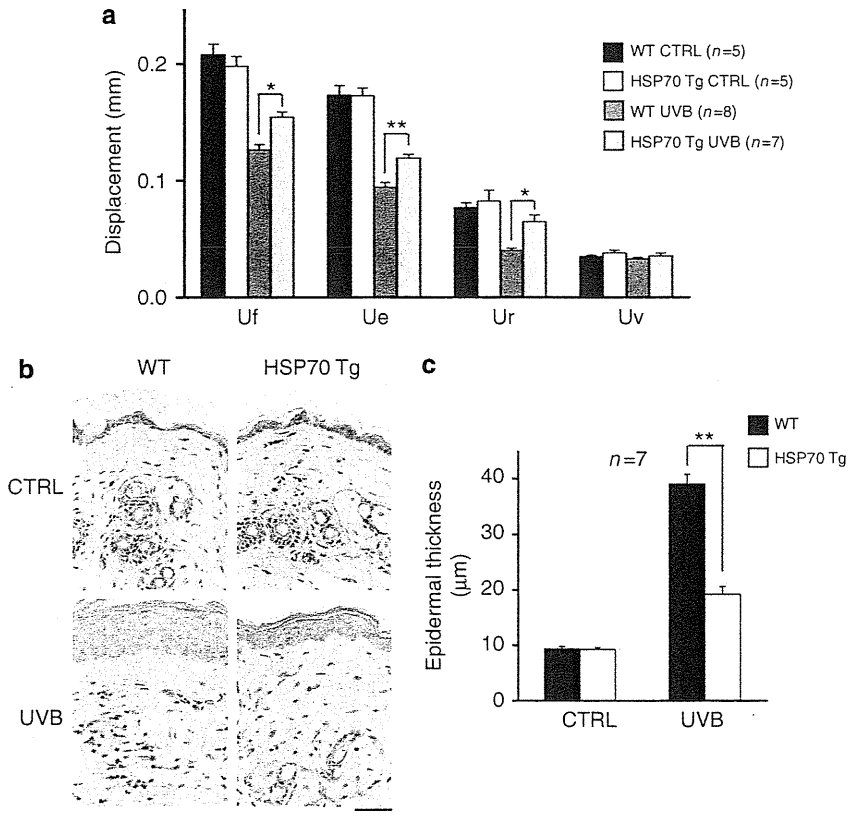

Figure 4. UVB-induced decrease in skin elasticity and epidermal hyperplasia in transgenic mice expressing heat shock protein 70 (HSP70). Transgenic mice expressing HSP70 (HSP70 Tg) and wild-type mice (WT) were irradiated with UVB as described in the legend of Figure 3. The skin elasticity (**a**) and epidermal thickness (**b**, **c**) were measured and shown as described in the legend of Figure 2. Values are mean ± SEM. $^{**}P<0.01$; $^{*}P<0.05$. CTRL, control.

were used in the study to examine the wrinkle formation. On the other hand, transgenic mice are useful to examine the role of specific proteins in biological responses. For this reason, we studied the role of HSPs on wrinkle formation using heat treatment of hairless mice, whereas the mechanism for the protective role of HSP70 on wrinkle formation was examined in transgenic mice expressing HSP70.

It was previously reported that more severe heat treatment conditions (e.g., 43 °C for 30 or 90 minutes) than those in this study (42 °C for 5 minutes) causes skin damage such as wrinkle formation and activation of MMPs *in vivo* (Cho *et al.*, 2008, 2009; ; Kim *et al.*, 2009; Shin *et al.*, 2012). We confirmed that heat treatment of mouse skin under severe conditions (43, 44, or 45 °C for 5 minutes) but not under mild conditions (42 °C for 5 minutes) caused an increase in the amount of MMP-13 (data not shown). We also observed an increase in the amounts and/or activities of MMP-2, MMP-9, and elastase in mouse skin by heat treatment of severe conditions (data not shown). On the other hand, we found that treatment of mouse skin at 42 °C or higher for 5 minutes clearly induced the expression of HSP70 (Figure 1 and data not shown). As the purpose of this study is to examine the protective role of HSP70 induced by heat treatment on the UVB-induced wrinkle formation, we used the mild heat treatment conditions (42 °C for 5 minutes). However, it should be noted that severe heat treatment damages the skin even without concomitant exposure to UVB.

We found that mild heat treatment of the dorsal skin of hairless mice suppressed UVB-induced wrinkle formation, and decrease in skin elasticity and epidermal hyperplasia. This is an evidence showing that mild heat treatment protects against UVB-induced wrinkle formation. Furthermore, the UVB-induced decrease in skin elasticity and epidermal hyperplasia was less apparent in transgenic mice expressing HSP70 compared with wild-type mice, suggesting that the mild heat treatment suppresses UVB-induced wrinkle formation through the induction of HSP70 expression.

UVB-induced wrinkle formation is mediated by a complex mechanism involving damage to the ECM and cell death, and the resulting inflammatory responses both in the epidermis and dermis. We showed here that exposure to UVB radiation caused skin fibroblast cell death and that this was suppressed in transgenic mice expressing HSP70. We also showed that reactive oxygen species-induced cell death was suppressed in HSP70-overexpressing skin fibroblasts compared with control fibroblasts cultured *in vitro*. Similar results were observed for keratinocytes in our previous paper (Matsuda *et al.*, 2010). We also found that compared with wild-type mice, the infiltration of inflammatory cells (macrophages and neutrophils) after long-term repeated UVB irradiation of animals was suppressed in transgenic mice expressing HSP70. We previously reported that a single UVB irradiation of wild-type mice decreased the skin level of IκB-α (an inhibitor of NF-κB) and increased proinflammatory cytokines and chemokines in the

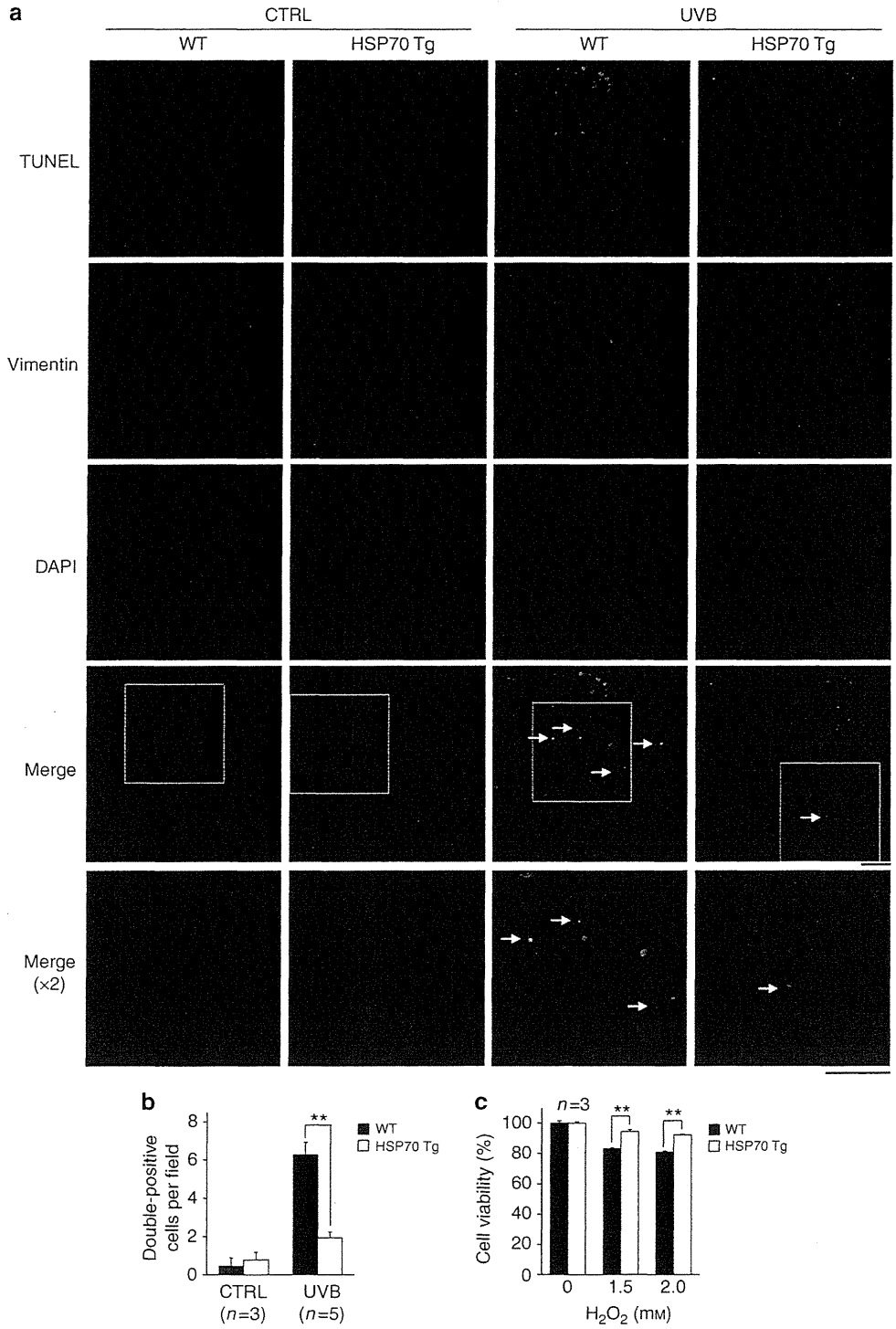

Figure 5. UVB-induced fibroblast cell death in transgenic mice expressing heat shock protein 70 (HSP70). (**a**, **b**) Transgenic mice expressing HSP70 (HSP70 Tg) and wild-type mice (WT) were irradiated with 180 mJ cm^{-2} UVB, and the dorsal skin was removed after 24 hours. (**a**) Sections were subjected to TUNEL assay, immunohistochemical analysis with antibody against vimentin, and 4,6-diamidino-2-phenylindole dihydrochloride (DAPI) staining (double-positive cells are shown by arrows; bar = 50 μm). (**b**) The number of double-positive cells (TUNEL and vimentin expression) was counted. (**c**) Primary cultures of skin fibroblasts prepared from HSP70 Tg and WT were treated with the indicated concentrations of hydrogen peroxide for 1 hour and cultured for 23 hours. Cell viability was determined by the 3-(4,5-dimethylthiazol-2-yl)-2,5-diphenyl tetrazolium bromide method. Values are mean ± SEM. $^{**}P < 0.01$. CTRL, control.

skin, and that these inflammatory responses were suppressed in transgenic mice expressing HSP70 (Matsuda *et al.*, 2010). Taken together, these results suggest that the cytoprotective and anti-inflammatory activities of HSP70 contribute to the suppression of UVB-induced phenomena related to wrinkle formation (decrease in skin elasticity and epidermal

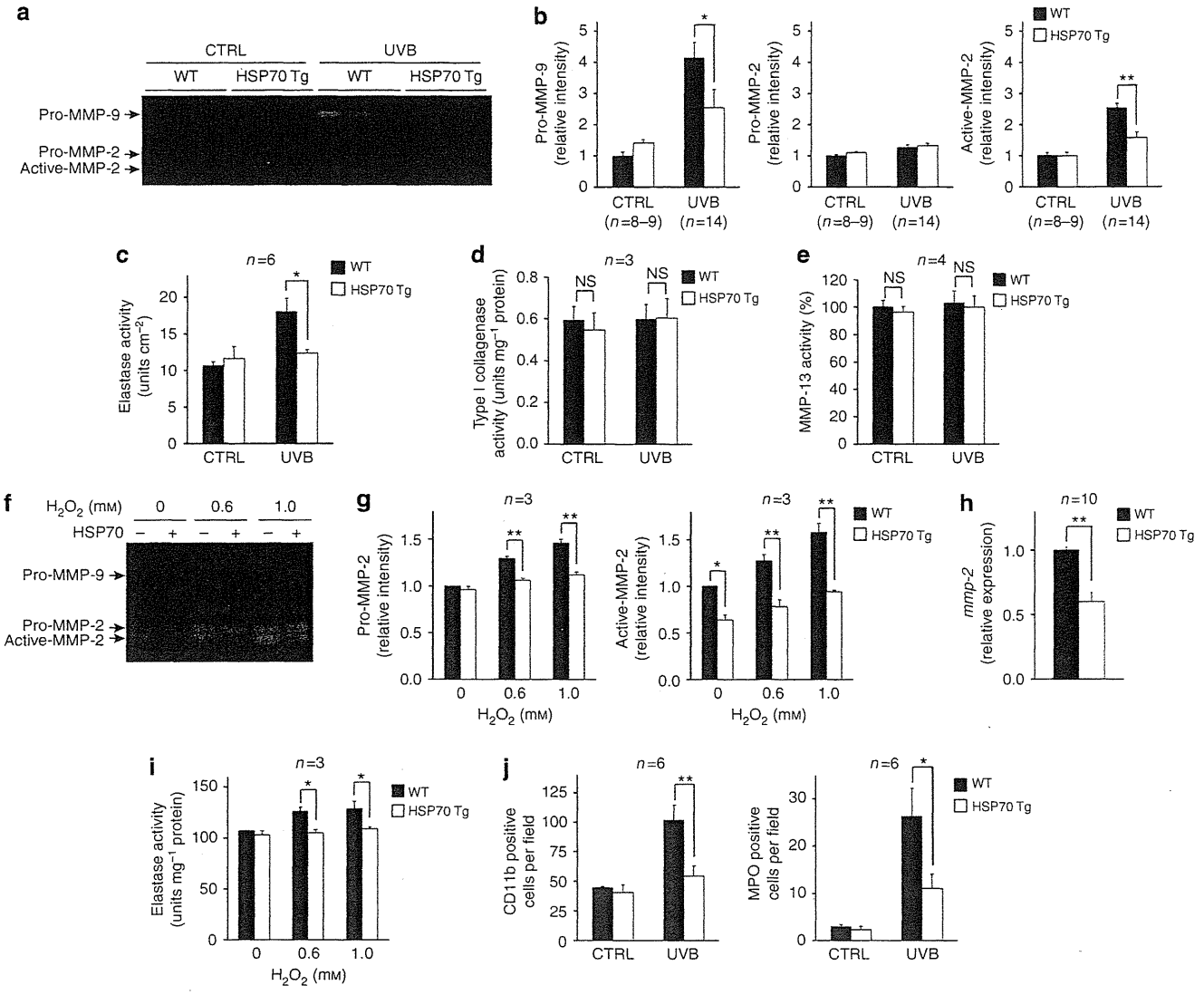

Figure 6. Effect of heat shock protein 70 (HSP70) overexpression on matrix metalloproteinases (MMPs) and elastase activities. (**a–e**, **j**) Mice were irradiated with UVB as described in the legend of Figure 3. (**f–i**) Primary skin fibroblasts were treated with hydrogen peroxide as described in the legend of Figure 5. Dorsal skin extracts (**a**) or culture media (**f**) were subjected to gelatin zymography assay, and the band intensity was determined (**b**, **g**). Elastase (**c**), type I collagenase (**d**), or MMP-13 (**e**) activity in dorsal skin extracts or elastase activity in cells (**i**) was measured. The messenger RNA expression was analyzed (**h**). The dorsal skin was subjected to immunohistochemical analysis for CD11b or myeloperoxidase, and the number of positive cells was counted (**j**). Values are mean ± SEM. $^{**}P<0.01$; $^{*}P<0.05$. CTRL, control; NS, not significant; WT, wild type.

hyperplasia) in transgenic mice expressing HSP70 and wild-type mice exposed to heat treatment.

Immunohistochemical analysis suggested that the level of type I collagen was decreased by UVB irradiation in control mice and that this decrease was partially suppressed in mice concomitantly exposed to mild heat treatment, or in transgenic mice expressing HSP70. This analysis also showed that fine basal membrane of the epidermis and collagen and elastic fibers were disrupted by UVB irradiation; this damage was partially suppressed in mice concomitantly exposed to mild heat treatment or in transgenic mice expressing HSP70. We also found that the activities of MMP-2, MMP-9, and elastase were increased by UVB irradiation and that these activities were lower in UVB-treated transgenic mice expressing HSP70 than in wild-type mice. These results suggest that MMP-2, MMP-9, and elastase have important roles in the HSP70-dependent protection against UVB-induced disruption of the ECM. As the overexpression of HSP70 in primary cultures of skin fibroblasts suppressed the expression and activity of MMP-2 and the activity of elastase, HSP70 seems to directly suppress the expression and/or activity of these proteases. On the other hand, the expression of HSP70 did not affect the activity of MMP-9 in macrophage primary cultures, suggesting that the decreased MMP-9 activity in UVB-treated transgenic mice expressing HSP70 may be owing to the suppression of infiltration of inflammatory cells into the skin.

We recently found that the artificial expression of HSP70 suppresses melanin production both *in vivo* and *in vitro* (Hoshino *et al.*, 2010). We also reported that HSP70 expression suppresses both UVB-induced cellular and DNA damage

and production of reactive oxygen species (Matsuda *et al.*, 2010). As UV-induced modest melanin production has an important role in protecting the skin against UV-dependent damage (Kobayashi *et al.*, 1998), our results suggest that HSP70 inducers could serve as hypopigmenting agents (skin whitening agents) without worsening UV-induced skin damage. The results of this study suggest that such HSP70 inducers could also be beneficial for reducing UV-induced wrinkle formation.

MATERIALS AND METHODS

Animals

The experiments and procedures described here were performed in accordance with the Guide for the Care and Use of Laboratory Animals as adopted and promulgated by the National Institutes of Health, and were approved by the Animal Care Committee of Kumamoto University and Keio University.

UVB irradiation and heat treatment

Animals were exposed to UVB radiation with a double bank of UVB lamps (peak emission at 312 nm, VL-215LM lamp, Vilber Lourmat, Paris, France). This UV lamp mainly emits UVB but emits a small level of UVA. Animals were placed under deep anesthesia with chloral hydrate (250 mg kg^{-1}), and the fur (except in the case of hairless mice) was removed with electric clippers before the first UVB irradiation.

The dorsal skin of hairless mice was exposed to heated water at 42 °C or 37 °C (control) for 5 minutes for heat treatment.

Wrinkles were formed as a consequence of long-term, repeated exposure to UVB radiation (three times a week for 6 or 10 weeks) as described previously (Inomata *et al.*, 2003) with some modifications. Briefly, in the case of hairless mice, the initial dose of UVB was set at 36 mJ cm^{-2}, which was subsequently increased weekly to 54, 72, 90, 108, 126, 144, 162, and finally 180 mJ cm^{-2} (180 mJ cm^{-2}, both at week 9 and week 10; a total of 10 weeks). In the case of transgenic mice expressing HSP70 and the wild-type mice (C57/BL6), the initial dose was set at 36 mJ cm^{-2}, which was subsequently increased weekly to 54, 72, 108, 144, and 180 mJ cm^{-2} (a total of 6 weeks).

Wrinkle scoring, image analysis of skin replicas, and measurement of skin elasticity

Evaluation of wrinkle formation was performed by both visual wrinkle scoring and image analysis of skin replicas as described previously (Inomata *et al.*, 2003; Tsukahara *et al.*, 2004). Skin elasticity was measured with a Cutometer 575 meter (Courage + Khazaka) as described previously (Agache *et al.*, 1980; Elsner *et al.*, 1990; Tsukahara *et al.*, 2001).

Real-time reverse-transcriptase–PCR analysis

Total RNA was extracted from cultured cells using the RNeasy Fibrous Tissue Mini kit (Qiagen, Valencia, CA) according to the manufacturer's protocol. Real-time reverse-transcriptase–PCR analysis was performed as described (Hoshino *et al.*, 2010). The primer sequence would be provided on request.

Histological and immunohistochemical analyses and TUNEL assay

Histological examination (hematoxylin and eosin staining), immunohistochemical analysis, and TUNEL assay were performed as described (Matsuda *et al.*, 2010).

Gelatin zymography and measurement of enzyme activity

The proteolytic activity of MMP-2 and MMP-9 was assessed by SDS-PAGE using zymogram gels containing 0.1% (w/v) gelatin, as described previously (Taraboletti *et al.*, 2000). Elastase activity was measured using *N*-succinyl-tri-alanyl-p-nitroanilide (Peptide Institute, Osaka, Japan) as a substrate, as described previously (Tsukahara *et al.*, 2004). Type I collagenase activity or MMP-13 activity was measured using the type I collagenase assay kit (Primary Cell, Hokkaido, Japan) or the SensoLyte MMP-13 assay kit (AnaSpec, San Jose, CA), respectively.

Statistical analysis

All values are expressed as the mean ± SEM. Two-way analysis of variance followed by the Tukey's test was used to evaluate differences between more than two groups. Differences were considered to be significant for values of $P<0.05$.

CONFLICT OF INTEREST

The authors state no conflict of interest.

ACKNOWLEDGMENTS

This work was supported by Grants-in-Aid for Scientific Research from the Ministry of Health, Labor, and Welfare of Japan, as well as the Japan Science and Technology Agency and Grants-in-Aid for Scientific Research from the Ministry of Education, Culture, Sports, Science and Technology, Japan.

REFERENCES

Agache PG, Monneur C, Leveque JL *et al.* (1980) Mechanical properties and Young's modulus of human skin *in vivo*. *Arch Dermatol Res* 269:221–32

Aimes RT, Quigley JP (1995) Matrix metalloproteinase-2 is an interstitial collagenase. Inhibitor-free enzyme catalyzes the cleavage of collagen fibrils and soluble native type I collagen generating the specific 3/4- and 1/4-length fragments. *J Biol Chem* 270:5872–6

Chen H, Wu Y, Zhang Y *et al.* (2006) Hsp70 inhibits lipopolysaccharide-induced NF-kappaB activation by interacting with TRAF6 and inhibiting its ubiquitination. *FEBS Lett* 580:3145–52

Cho S, Lee MJ, Kim MS *et al.* (2008) Infrared plus visible light and heat from natural sunlight participate in the expression of MMPs and type I procollagen as well as infiltration of inflammatory cell in human skin *in vivo*. *J Dermatol Sci* 50:123–33

Cho S, Shin MH, Kim YK *et al.* (2009) Effects of infrared radiation and heat on human skin aging *in vivo*. *J Investig Dermatol Symp Proc* 14:15–9

Elsner P, Wilhelm D, Maibach HI (1990) Mechanical properties of human forearm and vulvar skin. *Br J Dermatol* 122:607–14

Hoshino T, Matsuda M, Yamashita Y *et al.* (2010) Suppression of melanin production by expression of HSP70. *J Biol Chem* 285:13254–63

Imokawa G (2009) Mechanism of UVB-induced wrinkling of the skin: paracrine cytokine linkage between keratinocytes and fibroblasts leading to the stimulation of elastase. *J Investig Dermatol Symp Proc* 14:36–43

Inomata S, Matsunaga Y, Amano S *et al.* (2003) Possible involvement of gelatinases in basement membrane damage and wrinkle formation in chronically ultraviolet B-exposed hairless mouse. *J Invest Dermatol* 120:128–34

Kessenbrock K, Plaks V, Werb Z (2010) Matrix metalloproteinases: regulators of the tumor microenvironment. *Cell* 141:52–67

Kim MS, Kim YK, Lee DH *et al.* (2009) Acute exposure of human skin to ultraviolet or infrared radiation or heat stimuli increases mast cell numbers and tryptase expression in human skin *in vivo*. *Br J Dermatol* 160: 393–402

Kobayashi N, Nakagawa A, Muramatsu T *et al.* (1998) Supranuclear melanin caps reduce ultraviolet induced DNA photoproducts in human epidermis. *J Invest Dermatol* 110:806–10

Krappmann D, Wegener E, Sunami Y *et al.* (2004) The IkappaB kinase complex and NF-kappaB act as master regulators of lipopolysaccharide-induced gene expression and control subordinate activation of AP-1. *Mol Cell Biol* 24:6488–500

Matsuda M, Hoshino T, Yamashita Y *et al.* (2010) Prevention of UVB radiation-induced epidermal damage by expression of heat shock protein 70. *J Biol Chem* 285:5848–58

Matsumura Y, Ananthaswamy HM (2004) Toxic effects of ultraviolet radiation on the skin. *Toxicol Appl Pharmacol* 195:298–308

Maytin EV, Wimberly JM, Kane KS (1994) Heat shock modulates UVB-induced cell death in human epidermal keratinocytes: evidence for a hyperthermia-inducible protective response. *J Invest Dermatol* 103:547–53

Morimoto RI, Santoro MG (1998) Stress-inducible responses and heat shock proteins: new pharmacologic targets for cytoprotection. *Nat Biotechnol* 16:833–8

Park KC, Kim DS, Choi HO *et al.* (2000) Overexpression of HSP70 prevents ultraviolet B-induced apoptosis of a human melanoma cell line. *Arch Dermatol Res* 292:482–7

Plumier JC, Ross BM, Currie RW *et al.* (1995) Transgenic mice expressing the human heat shock protein 70 have improved post-ischemic myocardial recovery. *J Clin Invest* 95:1854–60

Rabe JH, Mamelak AJ, McElgunn PJ *et al.* (2006) Photoaging: mechanisms and repair. *J Am Acad Dermatol* 55:1–19

Rijken F, Bruijnzeel PL (2009) The pathogenesis of photoaging: the role of neutrophils and neutrophil-derived enzymes. *J Investig Dermatol Symp Proc* 14:67–72

Schwartz E (1988) Connective tissue alterations in the skin of ultraviolet irradiated hairless mice. *J Invest Dermatol* 91:158–61

Shin MH, Seo JE, Kim YK *et al.* (2012) Chronic heat treatment causes skin wrinkle formation and oxidative damage in hairless mice. *Mech Ageing Dev* 133:92–8

Talwar HS, Griffiths CE, Fisher GJ *et al.* (1995) Reduced type I and type III procollagens in photodamaged adult human skin. *J Invest Dermatol* 105:285–90

Tang D, Kang R, Xiao W *et al.* (2007) The anti-inflammatory effects of heat shock protein 72 involve inhibition of high-mobility-group box 1 release and proinflammatory function in macrophages. *J Immunol* 179:1236–44

Taraboletti G, Sonzogni L, Vergani V *et al.* (2000) Posttranscriptional stimulation of endothelial cell matrix metalloproteinases 2 and 1 by endothelioma cells. *Exp Cell Res* 258:384–94

Trautinger F (2001) Heat shock proteins in the photobiology of human skin. *J Photochem Photobiol B* 63:70–7

Trautinger F, Kindas-Mugge I, Barlan B *et al.* (1995) 72-kD heat shock protein is a mediator of resistance to ultraviolet B light. *J Invest Dermatol* 105:160–2

Tsuji N, Moriwaki S, Suzuki Y *et al.* (2001) The role of elastases secreted by fibroblasts in wrinkle formation: implication through selective inhibition of elastase activity. *Photochem Photobiol* 74:283–90

Tsukahara K, Nakagawa H, Moriwaki S *et al.* (2004) Ovariectomy is sufficient to accelerate spontaneous skin ageing and to stimulate ultraviolet irradiation-induced photoageing of murine skin. *Br J Dermatol* 151:984–94

Tsukahara K, Takema Y, Moriwaki S *et al.* (2001) Selective inhibition of skin fibroblast elastase elicits a concentration-dependent prevention of ultraviolet B-induced wrinkle formation. *J Invest Dermatol* 117:671–7

Visse R, Nagase H (2003) Matrix metalloproteinases and tissue inhibitors of metalloproteinases: structure, function, and biochemistry. *Circ Res* 92:827–39

Weiss YG, Bromberg Z, Raj N *et al.* (2007) Enhanced heat shock protein 70 expression alters proteasomal degradation of IkappaB kinase in experimental acute respiratory distress syndrome. *Crit Care Med* 35: 2128–2138

Wilson N, McArdle A, Guerin D *et al.* (2000) Hyperthermia to normal human skin *in vivo* upregulates heat shock proteins 27, 60, 72i and 90. *J Cutan Pathol* 27:176–82

Zhao R, Bruning E, Rossetti D *et al.* (2009) Extracts from Glycine max (soybean) induce elastin synthesis and inhibit elastase activity. *Exp Dermatol* 18:883–6

Drug Metab. Pharmacokinet. 28 (2): 118–124 (2013).

Regular Article

Comparison of Pharmacokinetics between Loxoprofen and Its Derivative with Lower Ulcerogenic Activity, Fluoro-loxoprofen

Naoki YAMAKAWA[1,2], Shintaro SUEMASU[1,2], Hiroshi WATANABE[2], Kayoko TAHARA[1], Ken-ichiro TANAKA[2], Yoshinari OKAMOTO[2], Masami OHTSUKA[2], Toru MARUYAMA[2] and Tohru MIZUSHIMA[1,2,*]

[1]*Department of Analytical Chemistry, Faculty of Pharmacy, Keio University, Tokyo, Japan*
[2]*Faculty of Life Sciences, Kumamoto University, Kumamoto, Japan*

Full text of this paper is available at http://www.jstage.jst.go.jp/browse/dmpk

Summary: We recently reported that, compared to loxoprofen (LOX, an non-steroidal anti-inflammatory drug), the LOX derivative fluoro-loxoprofen (F-LOX) is less ulcerogenic but has similar anti-inflammatory activity. Our previous *in vitro* studies suggested that both LOX and F-LOX are pro-drugs, the active metabolites of which are their *trans*-alcohol forms. In this study, we compared the pharmacokinetics of F-LOX and LOX in rats. Overall, the pharmacokinetic characteristics of F-LOX, including the formation of metabolites *in vivo* and *in vitro*, were comparable to those of LOX. However, F-LOX disappeared from the plasma more rapidly than LOX, which could potentially explain its lower ulcerogenicity. However, we showed that F-LOX produced fewer gastric lesions than LOX, even when a higher plasma concentration of F-LOX was maintained. Similar to LOX, F-LOX was readily metabolized to its *trans*- and *cis*-alcohol forms, with a higher level of the *trans*-alcohol form being observed after oral or intravenous administration of the drug. The preferential formation of the *trans*-alcohol form was also observed after incubation of F-LOX with rat liver homogenates *in vitro*. These results suggest that, similar to LOX, F-LOX acts as a pro-drug and that there is a metabolic system that selectively produces its active metabolite.

Keywords: loxoprofen; pharmacokinetics; liver homogenates; gastric lesions; rat

Introduction

Non-steroidal anti-inflammatory drugs (NSAIDs) comprise a useful family of therapeutics,[1] the actions of which are mediated *via* an inhibitory effect on cyclooxygenase (COX), an enzyme which is essential for the synthesis of inflammatory prostaglandins (PGs). However, NSAID use is also associated with gastrointestinal complications.[2–4] Given that PGs have a strong protective effect on the gastric mucosa, it was believed that NSAIDs induce gastric lesions only through the inhibition of COX. However, the increased incidence of gastrointestinal lesions and the decrease in PG levels induced by NSAIDs do not always occur in parallel,[5,6] suggesting that the former effect involves additional mechanisms. We have recently demonstrated that NSAIDs induce cell death in cultured gastric mucosal cells and at the gastric mucosa in a manner independent of COX inhibition but dependent on their membrane permeabilizing activity.[7–13] Furthermore, we suggested that both COX inhibition and gastric mucosal cell death are required for the formation of NSAID-induced gastric lesions.[11,14]

COX-1 and COX-2 are responsible for the majority of COX activity at the gastric mucosa and in tissues undergoing inflammation, respectively,[15,16] and a greatly reduced incidence of gastroduodenal lesions has been reported following treatment with selective COX-2 inhibitors (such as celecoxib and rofecoxib).[17,18] However, a recently raised concern regarding the use of selective COX-2 inhibitors involves the associated risk of cardiovascular thrombotic events.[19] This may be due to the fact that prostacyclin, a potent anti-aggregator of platelets and a vasodilator, is mainly produced by COX-2. Therefore, NSAIDs exhibiting gastrointestinal safety, other than selective COX-2 inhibitors, need to be developed. Based on our findings, we proposed that NSAIDs with lower membrane permeabilization activity would be easy on the stomach even in the absence of COX-2 selectivity.[9]

We screened for such NSAIDs from those used clinically and found that loxoprofen (LOX, **Fig. 1**) has lower membrane permeabilization activity and cytotoxicity than other NSAIDs.[20] LOX has been widely used in the Japanese market, because clinical studies have suggested that it is safer than other traditional NSAIDs,

Received May 24, 2012; Accepted July 31, 2012
J-STAGE Advance Published Date: August 14, 2012, doi:10.2133/dmpk.DMPK-12-RG-050
**To whom correspondence should be addressed:* Tohru MIZUSHIMA, Ph.D., *Department of Analytical Chemistry, Faculty of Pharmacy, Keio University, 1-5-30, Shibakoen, Minato-ku, Tokyo 105-8512, Japan. Tel. +81-3-5400-2628, Fax. +81-3-5400-2628, E-mail: mizushima-th@pha.keio.ac.jp*
This work was supported by Grants-in-Aid for Scientific Research from the Ministry of Health, Labour and Welfare of Japan, Grants-in-Aid for Scientific Research from the Ministry of Education, Culture, Sports, Science and Technology of Japan, and Grants-in-Aid from the Japan Science and Technology Agency.

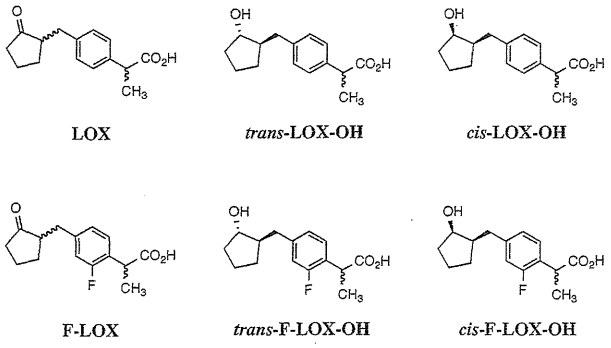

Fig. 1. Chemical structures of LOX, *trans*-LOX-OH, *cis*-LOX-OH, F-LOX, *trans*-F-LOX-OH and *cis*-F-LOX-OH

such as indomethacin.[21,22] LOX is a pro-drug, which is converted (by reduction of the cyclopentanone moiety) to its active *trans*-alcohol metabolite (*trans*-LOX-OH, **Fig. 1**) by multiple aldehyde-ketone reductases and carbonyl reductases only after absorption by the gastrointestinal tract.[23,24] We synthesized a series of LOX derivatives[25] and found that fluoro-loxoprofen (F-LOX, **Fig. 1**) has much lower membrane permeabilization and ulcerogenic activities than LOX but maintains similar anti-inflammatory activity.[26] We also suggested that the pro-drug property of LOX is maintained in F-LOX, based on the demonstration that the inhibitory activity of *trans*-F-LOX-OH (**Fig. 1**) on COX is more potent than that of F-LOX and its *cis*-alcohol metabolite (*cis*-F-LOX-OH, **Fig. 1**).[26] In this study, we compared the pharmacokinetics of LOX and F-LOX after oral or intravenous administration. Although some differences were observed, such as the more efficient absorption of F-LOX after its oral administration and its more rapid clearance from the plasma, the pharmacokinetic characters of F-LOX were basically comparable to those of LOX, including preferential metabolic formation of *trans*-F-LOX-OH rather than *cis*-F-LOX-OH. We therefore consider that F-LOX is likely to be a therapeutically beneficial NSAID due to its reduced gastric side effect.

Methods

Chemicals and animals: The sodium salts of LOX and F-LOX and their alcohol metabolites (*trans*-LOX-OH, *cis*-LOX-OH, *trans*-F-LOX-OH and *cis*-F-LOX-OH) were synthesized as reported previously[26] and their identities were confirmed by ^{1}H-NMR, ^{13}C-NMR, FAB-MS spectrum and elemental analysis (within ± 0.4% of the theoretical values). The purity of each tested compound was greater than 95% as assessed by high performance liquid chromatography (HPLC).

HPLC-grade acetonitrile was purchased from Sigma-Aldrich (St. Louis, MO). Wistar rats (6 weeks old, 180–200 g, male) were obtained from Kyudo Co. (Kumamoto, Japan). The experiments and procedures described here were carried out in accordance with the Guide for the Care and Use of Laboratory Animals as adopted and promulgated by the National Institutes of Health (Bethesda, MD), and were approved by the Animal Care Committee of Keio University and Kumamoto University.

HPLC analysis: The analytical HPLC with reverse-phase column (TSKgel Super-ODS, 150 × 4.6 mm, 2 µm, Tosoh Co., Tokyo, Japan) incorporated a Waters 2695 Alliance separation module and a Waters 2996 photodiode array detector (Waters, Milford, MA). Solvent A (0.1% trifluoroacetic acid in acetonitrile) and solvent B (0.1% trifluoroacetic acid in water) were used at a flow rate of 0.3 ml/min. After injection of the sample (0 min), the mobile phase was changed as follows: 35% solvent A (10 min), a linear gradient of 35–100% solvent A (3 min) and 100% solvent A (3 min). Detection was performed at an optical density of 220 nm.

Drug administration and pharmacokinetic analysis: Each compound was dissolved in saline and administered to rats at a dose of 20 mg/kg, orally or intravenously (*via* the tail vein). Tail vein blood samples (200 µl) were taken periodically (15, 30, 45, 60, 120 and 240 min after drug administration) into centrifuge tubes containing heparin. Samples were centrifuged immediately to obtain plasma. An aliquot (100 µl) of plasma was mixed with 500 µl of methanol to extract each compound and its metabolites. The suspension was centrifuged and the supernatant was analyzed by HPLC as described above.

Pharmacokinetic data analysis: A non-compartment model was used for the pharmacokinetic analysis. Each parameter, time of maximum concentration (T_{max}, min), maximum concentration (C_{max}, µg/ml), apparent elimination half-life ($t_{1/2}$, min), area under the concentration-time curve from time 0 to infinite times ($AUC_{0-\infty}$, µg/ml/min), mean residence time from time 0 to infinite times ($MRT_{0-\infty}$, min), total plasma clearance (CL_{tot}, ml/min/kg) and volume of distribution at the steady state (Vd_{ss}, ml), was calculated using the moment analysis program available on Microsoft Excel. The absolute oral bioavailability (F, %) was calculated using the following equation:

$$F(\%) = \frac{\text{Mean } AUC_{0-\infty,p.o.} \times \text{Dose}_{i.v.}}{\text{Mean } AUC_{0-\infty,i.v.} \times \text{Dose}_{p.o.}} \times 100$$

Drug treatment of rat liver homogenates *in vitro*: *In vitro* analysis for metabolic conversion of F-LOX and LOX was performed as described previously,[27] with some modifications. Rat livers were homogenized with PBS (1 ml PBS/g tissue) using a tissue homogenizer (Silent Crusher M, Heidolph, Germany). Each test compound in PBS (100 µl, 5 mg/ml) was mixed with 2 ml of the homogenates and incubated for various periods (10, 20, 30, 60, 120 and 240 min) at 37°C. The reaction was terminated by addition of 1.8 ml of methanol and the solution was centrifuged. The supernatant was analyzed by HPLC as described above.

Gastric damage assay: The gastric ulcerogenic response was examined as described previously,[25,28] with some modifications. Rats fasted for 18 h were orally administered LOX or F-LOX and, after 8 h, the animals were sacrificed, their stomachs were removed, and the areas of gastric mucosal lesions were measured by an observer unaware of the treatment that the animals had received. Calculation of the scores involved measuring the area of all the lesions in square millimeters and summing the values to give an overall lesion index.

Statistical analysis: All values are expressed as the mean ± S.D. or mean ± S.E.M. One-way or two-way analysis of variance (ANOVA) followed by the Tukey's test was used to evaluate differences among more than three groups. The Student's *t*-test for unpaired results was used for the evaluation of differences between two groups. Differences were considered to be significant for values of $p < 0.05$.

Results and Discussion

Pharmacokinetic analysis after oral or intravenous administration of LOX or F-LOX: We first compared the temporal profile of the plasma concentration following oral administration of

LOX and F-LOX (**Figs. 2A** and **2B**) and calculated the pharmacokinetic parameters based on moment analysis (non-compartment model) (**Table 1**). The pharmacokinetic characteristics of LOX (**Fig. 2**) were basically similar to those described previously,[27] and in general, the pharmacokinetic characteristics of F-LOX were comparable to those of LOX, as described below.

The C_{max} of F-LOX was significantly higher than that of LOX (**Table 1**), suggesting that F-LOX was absorbed more rapidly at the gastrointestinal mucosa. However, F and T_{max} values were not different between both F-LOX and LOX (**Table 1**). This may be due to the fact that the clearance of F-LOX is faster than LOX (see below).

The plasma level of F-LOX following oral administration (at 2 or 4 h) was lower than that of LOX (**Figs. 2A** and **2B**) and the $MRT_{0-\infty}$ and $t_{1/2}$ of the former drug were shorter (**Table 1**). We concluded that F-LOX was cleared from the plasma more rapidly than LOX. The $AUC_{0-\infty}$ of F-LOX following oral administration was smaller than that of LOX (**Table 1**).

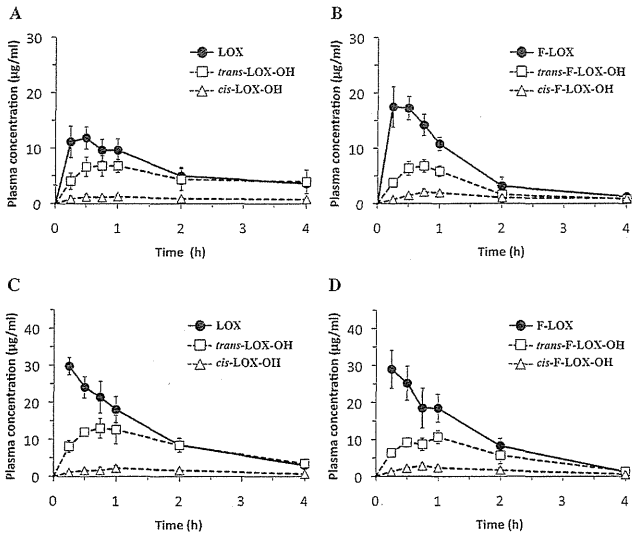

Fig. 2. Plasma concentrations of LOX and F-LOX and their metabolites following their oral or intravenous administration
Rats were administered LOX (A, C) or F-LOX (B, D) orally (A, B) or intravenously (C, D). The plasma concentration of each form of the drugs was monitored as described in Methods. Values are mean ± S.D. (n = 4–6).

We also monitored the temporal profile of the plasma concentrations of metabolites of LOX or F-LOX (*trans*-LOX-OH and *cis*-LOX-OH or *trans*-F-LOX-OH and *cis*-F-LOX-OH) after their oral administration and found that, similar to LOX, F-LOX was readily metabolized (**Figs. 2A** and **2B**). As previously described,[24,27,29] a relatively higher plasma level of *trans*-LOX-OH than *cis*-LOX-OH was observed (**Fig. 2A**). Similar results were observed for F-LOX (**Fig. 2B**). It is well known that LOX is metabolized to *trans*- or *cis*-LOX-OH with a stereoselectivity and multiple enzymes are involved in this stereoselectivity in humans.[24,30] Results in this study suggest that the system for this stereoselective reduction is common between rats and humans, which was suggested by the previous paper.[31,32] The C_{max} of *trans*-F-LOX-OH (active metabolite) after oral administration of F-LOX was similar to that of LOX (**Table 1**). However, the $t_{1/2}$ and and $AUC_{0-\infty}$ of *trans*-F-LOX-OH were shorter and smaller, respectively, than those of LOX (**Table 1**). We also calculated each pharmacokinetic parameter of *cis*-LOX-OH and *cis*-F-LOX-OH (**Table 1**); however, as the plasma level of each *cis*-OH form was very low, the accuracy of these results is debatable.

We also compared the plasma concentration-time profiles of LOX and F-LOX following their intravenous administration (**Figs. 2C** and **2D**). As in the case of oral administration, the $MRT_{0-\infty}$ and $t_{1/2}$ of F-LOX were shorter than those of LOX (**Table 1**), confirming the more rapid plasma clearance of the former drug. Compared to LOX, CL_{tot} of F-LOX after its intravenous administration tended to be higher, although this difference was not statistically significant (**Table 1**). The preferential conversion of F-LOX or LOX to its *trans*-OH rather than *cis*-OH form was also confirmed following intravenous administration (**Figs. 2C** and **2D**).

Pharmacokinetic analysis after administration of the *trans*- and *cis*-OH forms of LOX and F-LOX: We next compared the plasma concentration-time profile of each form of LOX and F-LOX after oral or intravenous administration of the *trans*- or

Table 1. Pharmacokinetic parameters after oral (*p.o.*, upper) or intravenous (i.v., lower) administration of LOX or F-LOX

Pharmacokinetic parameters	Unit	LOX *p.o.* (20.0 mg/kg)			F-LOX *p.o.* (21.3 mg/kg)		
		LOX	*trans*-LOX-OH	*cis*-LOX-OH	F-LOX	*trans*-F-LOX-OH	*cis*-F-LOX-OH
T_{max}	min	20 ± 9	45 ± 15	50 ± 17	20 ± 8.7	45 ± 0	70 ± 43
C_{max}	μg/ml	13.7 ± 1.9	8.3 ± 0.5	1.5 ± 0.2	19.5 ± 1.4*	6.5 ± 1.2	2.4 ± 0.3*
$t_{1/2}$	min	127 ± 32	373 ± 149	332 ± 100	59 ± 11*	105 ± 20*	132 ± 34*
$AUC_{0-\infty}$	μg/ml·min	2,419 ± 390	4,133 ± 1,908	827 ± 456	1,689 ± 186*	1,032 ± 34*	611 ± 184
$MRT_{0-\infty}$	min	192 ± 45	548 ± 217	577 ± 278	94 ± 19*	167 ± 28*	240 ± 47
F	%	61	—	—	51	—	—

Pharmacokinetic parameters	Unit	LOX i.v. (20.0 mg/kg)			F-LOX i.v. (21.3 mg/kg)		
		LOX	*trans*-LOX-OH	*cis*-LOX-OH	F-LOX	*trans*-F-LOX-OH	*cis*-F-LOX-OH
T_{max}	min	—	38 ± 8	49 ± 6	—	60 ± 0	75 ± 26
C_{max}	μg/ml	—	13.5 ± 2	2.4 ± 0.6	—	10.7 ± 1.5	3.5 ± 0.3*
$t_{1/2}$	min	68 ± 5	109 ± 19	114 ± 20	48 ± 6*	85 ± 5	71 ± 3*
$AUC_{0-\infty}$	μg/ml·min	3,227 ± 336	2,412 ± 172	445 ± 45	2,775 ± 324	1,502 ± 346**	487 ± 65
$MRT_{0-\infty}$	min	98 ± 8	173 ± 24	186 ± 24	72 ± 8**	134 ± 4*	129 ± 7**
CL_{tot}	ml/min/kg	6.3 ± 0.7	—	—	7.3 ± 0.9	—	—
Vd_{ss}	ml	609 ± 49	—	—	530 ± 108	—	—

Data in **Figure 2** were used to calculate each pharmacokinetic parameter as described in Methods. Values are mean ± S.D. (n = 4–6). *$p < 0.05$, **$p < 0.01$ (*vs.* LOX and its metabolites).

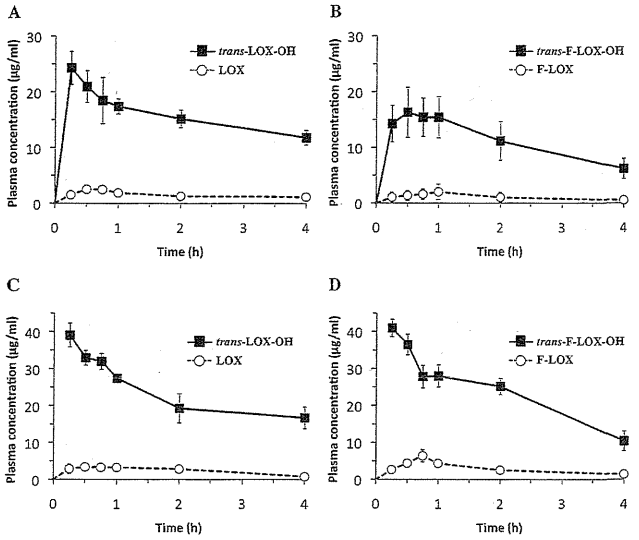

Fig. 3. Plasma concentration of *trans*-LOX-OH and *trans*-F-LOX-OH and their metabolites following their oral or intravenous administration
Rats were administered *trans*-LOX-OH (A, C) or *trans*-F-LOX-OH (B, D) orally (A, B) or intravenously (C, D). The plasma concentration of each form of the drugs was monitored. Values are mean ± S.D. ($n = 4$–6).

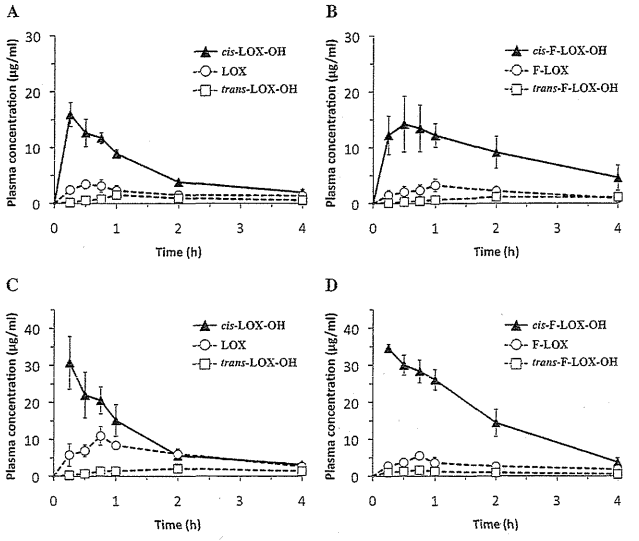

Fig. 4. Plasma concentration of *cis*-LOX-OH and *cis*-F-LOX-OH and their metabolites following their oral or intravenous administration
Rats were administered *cis*-LOX-OH (A, C) or *cis*-F-LOX-OH (B, D) orally (A, B) or intravenously (C, D). The plasma concentration of each form of the drugs was monitored. Values are mean ± S.D. ($n = 4$–6).

Table 2. Pharmacokinetic parameters after oral (*p.o.*, upper) or intravenous (i.v., lower) administration of the *trans*-OH form of LOX or F-LOX

Pharmacokinetic parameters	Unit	*trans*-LOX-OH *p.o.* (20.0 mg/kg)			*trans*-F-LOX-OH *p.o.* (21.3 mg/kg)		
		trans-LOX-OH	LOX	*cis*-LOX-OH	*trans*-F-LOX-OH	F-LOX	*cis*-F-LOX-OH
T_{max}	min	15 ± 0	35 ± 7	N.D.	38 ± 13	60 ± 0	N.D.
C_{max}	μg/ml	25.0 ± 3	2.9 ± 0.4	N.D.	16.5 ± 3.7*	2.0 ± 1.2	N.D.
$t_{1/2}$	min	227 ± 28	149 ± 8	N.D.	145 ± 20*	91 ± 52	N.D.
$AUC_{0-\infty}$	μg/ml·min	7,229 ± 762	558 ± 165	N.D.	3,889 ± 964**	360 ± 276	N.D.
$MRT_{0-\infty}$	min	336 ± 39	233 ± 13	N.D.	216 ± 25**	154 ± 74	N.D.
F	%	81	—	—	60	—	—

Pharmacokinetic parameters	Unit	*trans*-LOX-OH i.v. (20.0 mg/kg)			*trans*-F-LOX-OH i.v. (21.3 mg/kg)		
		trans-LOX-OH	LOX	*cis*-LOX-OH	*trans*-F-LOX-OH	F-LOX	*cis*-F-LOX-OH
T_{max}	min	—	53 ± 40	N.D.	—	45 ± 0	N.D.
C_{max}	μg/ml	—	4.2 ± 0.5	N.D.	—	6.4 ± 1.4*	N.D.
$t_{1/2}$	min	193 ± 36	75 ± 16	N.D.	129 ± 27*	100 ± 21	N.D.
$AUC_{0-\infty}$	μg/ml·min	9,920 ± 1,809	538 ± 93	N.D.	7,611 ± 999	662 ± 103	N.D.
$MRT_{0-\infty}$	min	282 ± 52	99 ± 12	N.D.	174 ± 25*	99 ± 8	N.D.
CL_{tot}	ml/min/kg	2.1 ± 0.4	—	—	2.7 ± 0.4	—	—
Vd_{ss}	ml	570 ± 42	—	—	456 ± 10**	—	—

Data in **Figure 3** were used to calculate each pharmacokinetic parameter as described in Methods. Values are mean ± S.D. ($n = 4$–6). *$p < 0.05$, **$p < 0.01$ (*vs.* LOX and its metabolites). N.D., not detected.

cis-OH form. As shown in **Figures 3** and **4**, LOX was detected after oral or intravenous administration of *trans*-LOX-OH or *cis*-LOX-OH. *trans*-LOX-OH was detected after oral or intravenous administration of *cis*-LOX-OH; however, *cis*-LOX-OH was not detected after oral or intravenous administration of *trans*-LOX-OH (**Figs. 3** and **4**). These results are consistent with those reported previously.[33] Similar results were also observed for F-LOX (**Figs. 3** and **4**), suggesting that there is a metabolic system which converts *trans*- or *cis*-F-LOX-OH to F-LOX. Our results also support the idea that the metabolic system converts F-LOX preferentially to *trans*-F-LOX-OH rather than to *cis*-F-LOX-OH, the assumption being that *trans*-F-LOX-OH is produced from *cis*-F-LOX-OH *via* F-LOX.

The data in **Table 2** show that the C_{max} of *trans*-F-LOX-OH was less than that of *trans*-LOX-OH following their oral administration, suggesting that the absorption of *trans*-F-LOX-OH was slower, in contrast to the situation with the ketone forms of these NSAIDs (**Table 1**). However, the $t_{1/2}$ and $MRT_{0-\infty}$ of *trans*-F-LOX-OH were shorter than those of *trans*-LOX-OH following both oral and intravenous administration (**Table 2**), this being consistent with what is observed in the case of their ketone forms (**Table 1**).

The data in **Table 3** show that the pharmacokinetic characteristics of *cis*-F-LOX-OH, relative to *cis*-LOX-OH, differed from those of F-LOX and *trans*-F-LOX-OH. For example, the $MRT_{0-\infty}$ of *cis*-F-LOX-OH was longer than that of *cis*-LOX-OH after oral administration and $AUC_{0-\infty}$ or CL_{tot} of *cis*-F-LOX-OH was higher or lower than that of *cis*-LOX-OH after intravenous administration (**Table 3**). However, as the *cis*-OH forms of F-LOX and LOX are inactive in terms of COX-inhibition,[26] these results may not be clinically or pharmacologically relevant.

Table 3. Pharmacokinetic parameters after oral (*p.o.*, upper) or intravenous (i.v., lower) administration of the *cis*-OH form of LOX or F-LOX

Pharmacokinetic parameters	Unit	*cis*-LOX-OH *p.o.* (20.0 mg/kg)			*cis*-F-LOX-OH *p.o.* (21.3 mg/kg)		
		cis-LOX-OH	LOX	*trans*-LOX-OH	*cis*-F-LOX-OH	F-LOX	*trans*-F-LOX-OH
T_{max}	min	15 ± 0	34 ± 6	60 ± 0	38 ± 13	56 ± 6	60 ± 0
C_{max}	μg/ml	15.2 ± 1.5	3.4 ± 0.7	1.5 ± 0.4	14.6 ± 3.8	3.4 ± 0.9	1.4 ± 0.4
$t_{1/2}$	min	74 ± 9	200 ± 53	143 ± 37	123 ± 34	93 ± 30*	93 ± 10.2
$AUC_{0-\infty}$	μg/ml·min	1,557 ± 85	926 ± 314	317 ± 97	3,037 ± 1,076	593 ± 260	372 ± 157
$MRT_{0-\infty}$	min	113 ± 13	383 ± 158	247 ± 53	191 ± 46*	165 ± 38	236 ± 50
F	%	59	—	—	75	—	—

Pharmacokinetic parameters	Unit	*cis*-LOX-OH i.v. (20.0 mg/kg)			*cis*-F-LOX-OH i.v. (21.3 mg/kg)		
		cis-LOX-OH	LOX	*trans*-LOX-OH	*cis*-F-LOX-OH	F-LOX	*trans*-F-LOX-OH
T_{max}	min	—	49 ± 6	101 ± 32	—	45 ± 0	45 ± 0
C_{max}	μg/ml	—	11.2 ± 1.7	2.4 ± 0.5	—	5.6 ± 0.9*	1.7 ± 0.3
$t_{1/2}$	min	68 ± 1	98 ± 7	175 ± 89	69 ± 8	111 ± 31	176 ± 53
$AUC_{0-\infty}$	μg/ml·min	2,785 ± 429	1,707 ± 70	757 ± 402	4,387 ± 602*	932 ± 183**	442 ± 124
$MRT_{0-\infty}$	min	94 ± 2	164 ± 7	312 ± 123	100 ± 11	189 ± 43	334 ± 115
CL_{tot}	ml/min/kg	7.4 ± 1.3	—	—	4.6 ± 0.6*	—	—
Vd_{ss}	ml	697 ± 138	—	—	460 ± 27*	—	—

Data in **Figure 4** were used to calculate each pharmacokinetic parameter as described in Methods. Values are mean ± S.D. (n = 4–6). *p < 0.05, **p < 0.01 (*vs.* LOX and its metabolites).

Metabolic conversion of F-LOX and LOX *in vitro*: It has previously been reported that LOX is metabolized in the liver *in vivo* and that the conversion of LOX to *trans*- or *cis*-LOX-OH can be reproduced *in vitro* using rat liver homogenates.[34] Using this system, we examined the conversion of F-LOX to its *trans*- or *cis*-OH form *in vitro*. We first showed that incubation of LOX with rat liver homogenates produced a higher level of *trans*-LOX-OH than *cis*-LOX-OH (**Fig. 5A**). Although both *trans*-LOX-OH and *cis*-LOX-OH were more stable than LOX in this system, incubation of *trans*-LOX-OH or *cis*-LOX-OH with the homogenates generated only LOX or both LOX and *trans*-LOX-OH, respectively (**Figs. 5A–5C**). These results are consistent with those previously reported.[34] As shown in **Figures 5D–5F**, results obtained with F-LOX were essentially similar to those seen with LOX. Incubation of F-LOX with rat liver homogenates produced a higher level of *trans*-F-LOX-OH than *cis*-F-LOX-OH (**Fig. 5D**). Given that the formation of *trans*- or *cis*-F-LOX-OH was associated with concomitant loss of F-LOX and the sum of F-LOX, *trans*-F-LOX-OH and *cis*-F-LOX-OH was consistent throughout the incubation (**Fig. 5D**), it appears that the homogenates metabolized F-LOX selectively to *trans*-F-LOX-OH and *cis*-F-LOX-OH. Incubation of *trans*-F-LOX-OH or *cis*-F-LOX-OH with the homogenates generated F-LOX and the conversion from *trans*-F-LOX-OH was more efficient that from *cis*-F-LOX-OH (**Figs. 5E** and **5F**). Furthermore, although the incubation of *cis*-F-LOX-OH with the homogenates generated *trans*-F-LOX-OH, the opposite did not occur (**Figs. 5E** and **5F**). These results correlate well with the *in vivo* findings illustrated in **Figures 3** and **4**. The results in **Figure 5** suggest that there is a metabolic system that converts F-LOX and LOX preferentially to their *trans*-OH rather than *cis*-OH forms.

Results in **Figure 5** show that the disappearance rate of F-LOX was similar to that of LOX. Therefore, the more rapid clearance of F-LOX than LOX that was observed *in vivo* could not be explained by its metabolic conversion in the liver. The examination of the urinary clearance and protein binding would be required to understand the mechanism for the difference in pharmacokinetics between the two drugs.

Production of gastric lesions by F-LOX and LOX: We have previously reported that F-LOX produces fewer gastric lesions than

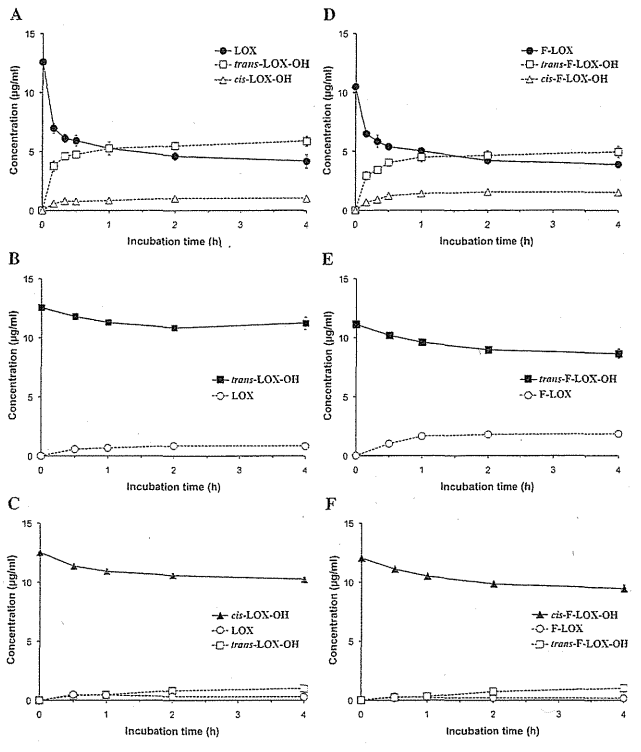

Fig. 5. Metabolic conversion of LOX and F-LOX and their metabolites in rat liver homogenates *in vitro*
Each drug [LOX (A), *trans*-LOX-OH (B), *cis*-LOX-OH (C), F-LOX (D), *trans*-F-LOX-OH (E) and *cis*-F-LOX-OH (F)] (500 μg) was incubated with rat liver homogenates at 37°C. Samples were obtained periodically and the amount of each form of LOX or F-LOX was determined. Values are mean ± S.E.M. (n = 3).

LOX in rats, and proposed that this lower ulcerogenic activity of F-LOX is due to its lower membrane permeabilization activity.[26] However, given that the results demonstrate that F-LOX and its active metabolite (*trans*-F-LOX-OH) disappear from the plasma more rapidly than LOX, it is also possible that the lower ulcerogenic activity of F-LOX is due to its lower plasma level after a

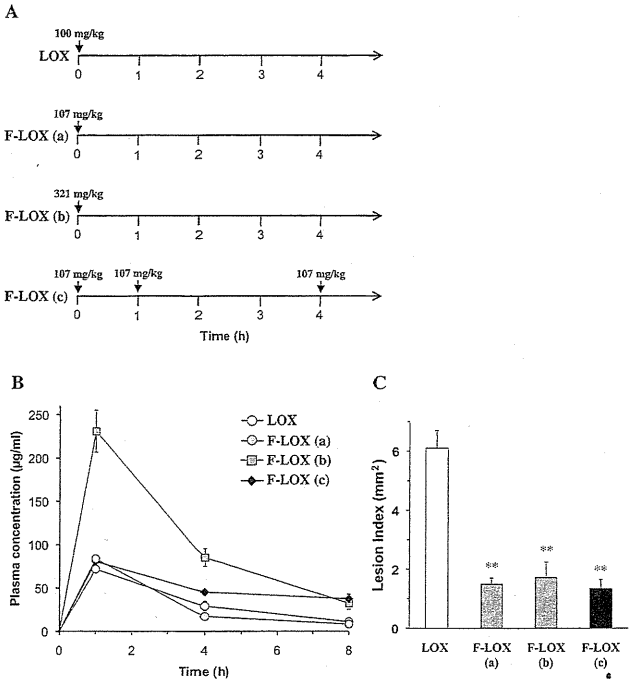

Fig. 6. Production of gastric lesions by LOX or F-LOX
The administration protocols for LOX or F-LOX are shown (A): rats were orally administered 100 mg/kg of LOX once only at time 0, 107 mg/kg of F-LOX once only at time 0 (a), 321 mg/kg of F-LOX once only at time 0 (b), or 107 mg/kg of F-LOX at 0, 1 and 4 h (c). The plasma concentration of LOX or F-LOX was monitored (B). Stomachs were removed after 8 h and scored for hemorrhagic damage (C). Values are mean ± S.E.M. ($n = 4$). $^{**}p < 0.01$ (*vs.* LOX).

single oral administration. To test this possibility, we performed the experiments illustrated in **Figure 6**. In this study, in order to keep the plasma concentration of F-LOX higher than that of LOX, rats were either administered a 3-fold higher dose of F-LOX than LOX or administered the same dose of F-LOX as LOX but at 3 time-points (0, 1 and 4 h) (**Fig. 6A**). As shown in **Figure 6B**, a consistently higher plasma concentration of F-LOX than LOX was achieved using these protocols. Administration of F-LOX produced fewer gastric lesions than LOX in all cases (**Fig. 6C**), strongly suggesting that the lower ulcerogenic activity of the former drug cannot be explained by the differences in its pharmacokinetic characteristics. In other words, the lower ulcerogenic activity of F-LOX seems to be derived from other properties, such as its lower membrane permeabilization activity.

Conclusions: In this study, we compared the pharmacokinetics of F-LOX and LOX. Although some differences were observed, it should be noted that the pharmacokinetic characteristics of F-LOX are basically comparable to those of LOX. In particular, it is important to note that the metabolic conversion characteristics of the ketone, *trans*-OH- and *cis*-OH forms of LOX were maintained in F-LOX, given that the pro-drug properties of LOX are believed to play important roles in its clinically beneficial effects, including its potent anti-inflammatory action and low gastrointestinal side effect. Therefore, the results in this study confirm the idea that F-LOX is a LOX analog with reduced gastrointestinal side effects and suggest that it is likely to be a therapeutically safer NSAID.

References

1) Smalley, W. E., Ray, W. A., Daugherty, J. R. and Griffin, M. R.: Nonsteroidal anti-inflammatory drugs and the incidence of hospitalizations for peptic ulcer disease in elderly persons. *Am. J. Epidemiol.*, **141**: 539–545 (1995).
2) Hawkey, C. J.: Nonsteroidal anti-inflammatory drug gastropathy. *Gastroenterology*, **119**: 521–535 (2000).
3) Barrier, C. H. and Hirschowitz, B. I.: Controversies in the detection and management of nonsteroidal antiinflammatory drug-induced side effects of the upper gastrointestinal tract. *Arthritis Rheum.*, **32**: 926–932 (1989).
4) Fries, J. F., Miller, S. R., Spitz, P. W., Williams, C. A., Hubert, H. B. and Bloch, D. A.: Toward an epidemiology of gastropathy associated with nonsteroidal antiinflammatory drug use. *Gastroenterology*, **96**: 647–655 (1989).
5) Ligumsky, M., Golanska, E. M., Hansen, D. G. and Kauffman, G. J.: Aspirin can inhibit gastric mucosal cyclo-oxygenase without causing lesions in rat. *Gastroenterology*, **84**: 756–761 (1983).
6) Ligumsky, M., Sestieri, M., Karmeli, F., Zimmerman, J., Okon, E. and Rachmilewitz, D.: Rectal administration of nonsteroidal antiinflammatory drugs. Effect on rat gastric ulcerogenicity and prostaglandin E2 synthesis. *Gastroenterology*, **98**: 1245–1249 (1990).
7) Tanaka, K., Tomisato, W., Hoshino, T., Ishihara, T., Namba, T., Aburaya, M., Katsu, T., Suzuki, K., Tsutsumi, S. and Mizushima, T.: Involvement of intracellular Ca^{2+} levels in nonsteroidal anti-inflammatory drug-induced apoptosis. *J. Biol. Chem.*, **280**: 31059–31067 (2005).
8) Tsutsumi, S., Gotoh, T., Tomisato, W., Mima, S., Hoshino, T., Hwang, H. J., Takenaka, H., Tsuchiya, T., Mori, M. and Mizushima, T.: Endoplasmic reticulum stress response is involved in nonsteroidal anti-inflammatory drug-induced apoptosis. *Cell Death Differ.*, **11**: 1009–1016 (2004).
9) Tomisato, W., Tanaka, K., Katsu, T., Kakuta, H., Sasaki, K., Tsutsumi, S., Hoshino, T., Aburaya, M., Li, D., Tsuchiya, T., Suzuki, K., Yokomizo, K. and Mizushima, T.: Membrane permeabilization by non-steroidal anti-inflammatory drugs. *Biochem. Biophys. Res. Commun.*, **323**: 1032–1039 (2004).
10) Tomisato, W., Tsutsumi, S., Rokutan, K., Tsuchiya, T. and Mizushima, T.: NSAIDs induce both necrosis and apoptosis in guinea pig gastric mucosal cells in primary culture. *Am. J. Physiol. Gastrointest. Liver Physiol.*, **281**: G1092–G1100 (2001).
11) Aburaya, M., Tanaka, K., Hoshino, T., Tsutsumi, S., Suzuki, K., Makise, M., Akagi, R. and Mizushima, T.: Heme oxygenase-1 protects gastric mucosal cells against non-steroidal anti-inflammatory drugs. *J. Biol. Chem.*, **281**: 33422–33432 (2006).
12) Tsutsumi, S., Namba, T., Tanaka, K. I., Arai, Y., Ishihara, T., Aburaya, M., Mima, S., Hoshino, T. and Mizushima, T.: Celecoxib upregulates endoplasmic reticulum chaperones that inhibit celecoxib-induced apoptosis in human gastric cells. *Oncogene*, **25**: 1018–1029 (2006).
13) Namba, T., Hoshino, T., Tanaka, K., Tsutsumi, S., Ishihara, T., Mima, S., Suzuki, K., Ogawa, S. and Mizushima, T.: Up-regulation of 150-kDa oxygen-regulated protein by celecoxib in human gastric carcinoma cells. *Mol. Pharmacol.*, **71**: 860–870 (2007).
14) Tomisato, W., Tsutsumi, S., Hoshino, T., Hwang, H. J., Mio, M., Tsuchiya, T. and Mizushima, T.: Role of direct cytotoxic effects of NSAIDs in the induction of gastric lesions. *Biochem. Pharmacol.*, **67**: 575–585 (2004).
15) Kujubu, D. A., Fletcher, B. S., Varnum, B. C., Lim, R. W. and Herschman, H. R.: TIS10, a phorbol ester tumor promoter-inducible mRNA from Swiss 3T3 cells, encodes a novel prostaglandin synthase/cyclooxygenase homologue. *J. Biol. Chem.*, **266**: 12866–12872 (1991).
16) Xie, W. L., Chipman, J. G., Robertson, D. L., Erikson, R. L. and Simmons, D. L.: Expression of a mitogen-responsive gene encoding prostaglandin synthase is regulated by mRNA splicing. *Proc. Natl. Acad. Sci. USA*, **88**: 2692–2696 (1991).
17) Silverstein, F. E., Faich, G., Goldstein, J. L., Simon, L. S., Pincus, T., Whelton, A., Makuch, R., Eisen, G., Agrawal, N. M., Stenson, W. F., Burr, A. M., Zhao, W. W., Kent, J. D., Lefkowith, J. B., Verburg, K. M. and Geis, G. S.: Gastrointestinal toxicity with celecoxib vs nonsteroidal anti-inflammatory drugs for osteoarthritis and rheumatoid arthritis: the CLASS study: A randomized controlled trial. Celecoxib Long-term Arthritis Safety Study. *JAMA*, **284**: 1247–1255 (2000).
18) Bombardier, C., Laine, L., Reicin, A., Shapiro, D., Burgos, V. R., Davis, B., Day, R., Ferraz, M. B., Hawkey, C. J., Hochberg, M. C., Kvien, T. K. and Schnitzer, T. J.: Comparison of upper gastrointestinal toxicity of rofecoxib and naproxen in patients with rheumatoid arthritis. VIGOR Study Group. *N. Engl. J. Med.*, **343**: 1520–1528 (2000).
19) Mukherjee, D., Nissen, S. E. and Topol, E. J.: Risk of cardiovascular

events associated with selective COX-2 inhibitors. *JAMA*, **286**: 954–959 (2001).
20) Yamakawa, N., Suemasu, S., Kimoto, A., Arai, Y., Ishihara, T., Yokomizo, K., Okamoto, Y., Otsuka, M., Tanaka, K. and Mizushima, T.: Low direct cytotoxicity of loxoprofen on gastric mucosal cells. *Biol. Pharm. Bull.*, **33**: 398–403 (2010).
21) Misaka, E., Yamaguchi, T., Iizuka, Y., Kamoshida, K., Kojima, T., Kobayashi, K., Endo, Y., Misawa, Y., Lobayashi, S. and Tanaka, K.: Anti-inflammatory, Analgesic and Antipyretic Activities of Sodium 2-[4-(2-oxocyclopentan-1-ylmethyl)phenyl] Propionate Dihydrate (CS-600). *Pharmacometrics*, **21**: 753–771 (1981).
22) Kawano, S., Tsuji, S., Hayashi, N., Takei, Y., Nagano, K., Fusamoto, H. and Kamada, T.: Effects of loxoprofen sodium, a newly synthesized non-steroidal anti-inflammatory drug, and indomethacin on gastric mucosal haemodynamics in the human. *J. Gastroenterol. Hepatol.*, **10**: 81–85 (1995).
23) Sugimoto, M., Kojima, T., Asami, M., Iizuka, Y. and Matsuda, K.: Inhibition of prostaglandin production in the inflammatory tissue by loxoprofen-Na, an anti-inflammatory prodrug. *Biochem. Pharmacol.*, **42**: 2363–2368 (1991).
24) Ohara, H., Miyabe, Y., Deyashiki, Y., Matsuura, K. and Hara, A.: Reduction of drug ketones by dihydrodiol dehydrogenases, carbonyl reductase and aldehyde reductase of human liver. *Biochem. Pharmacol.*, **50**: 221–227 (1995).
25) Yamakawa, N., Suemasu, S., Matoyama, M., Tanaka, K.-i., Katsu, T., Miyata, K., Okamoto, Y., Otsuka, M. and Mizushima, T.: Synthesis and biological evaluation of loxoprofen derivatives. *Bioorg. Med. Chem.*, **19**: 3299–3311 (2011).
26) Yamakawa, N., Suemasu, S., Matoyama, M., Kimoto, A., Takeda, M., Tanaka, K., Ishihara, T., Katsu, T., Okamoto, Y., Otsuka, M. and Mizushima, T.: Properties and synthesis of 2-{2-fluoro (or bromo)-4-[(2-oxocyclopentyl)methyl]phenyl}propanoic acid: nonsteroidal anti-inflammatory drugs with low membrane permeabilizing and gastric lesion-producing activities. *J. Med. Chem.*, **53**: 7879–7882 (2010).
27) Koo, T. S., Kim, D. H., Ahn, S. H., Kim, K. P., Kim, I. W., Seo, S. Y., Suh, Y. G., Kim, D. D., Shim, C. K. and Chung, S. J.: Comparison of pharmacokinetics of loxoprofen and its active metabolites after an intravenous, intramuscular, and oral administration of loxoprofen in rats: evidence for extrahepatic metabolism. *J. Pharm. Sci.*, **94**: 2187–2197 (2005).
28) Suemasu, S., Tanaka, K., Namba, T., Ishihara, T., Katsu, T., Fujimoto, M., Adachi, H., Sobue, G., Takeuchi, K., Nakai, A. and Mizushima, T.: A role for HSP70 in protecting against indomethacin-induced gastric lesions. *J. Biol. Chem.*, **284**: 19705–19715 (2009).
29) Choo, K. S., Kim, I. W., Jung, J. K., Suh, Y. G., Chung, S. J., Lee, M. H. and Shim, C. K.: Simultaneous determination of loxoprofen and its diastereomeric alcohol metabolites in human plasma and urine by a simple HPLC-UV detection method. *J. Pharm. Biomed. Anal.*, **25**: 639–650 (2001).
30) Naganuma, H., Mochizuki, Y. and Kawahara, Y.: Study of pharmacokinetics following oral administration of loxprofen sodium (CS-600) in humans. *J. Clin. Ther. Med.*, **2**: 1219–1237 (1986).
31) Pawlowski, J. E., Huizinga, M. and Penning, T. M.: Cloning and sequencing of the cDNA for rat liver 3 alpha-hydroxysteroid/dihydrodiol dehydrogenase. *J. Biol. Chem.*, **266**: 8820–8825 (1991).
32) Deyashiki, Y., Ogasawara, A., Nakayama, T., Nakanishi, M., Miyabe, Y., Sato, K. and Hara, A.: Molecular cloning of two human liver 3 alpha-hydroxysteroid/dihydrodiol dehydrogenase isoenzymes that are identical with chlordecone reductase and bile-acid binder. *Biochem. J.*, **299**(Pt 2): 545–552 (1994).
33) Tanaka, Y.: Stereoselective metabolism studies on loxoprofen, a 2-arylpropionic acid nonsteroidal anti-inflammatory drug, and its role for the development as a prodrug. *Drug Metab. Pharmacokinet.*, **8**: 521–536 (1993).
34) Koo, T. S., Kim, D. H., Ahn, S. H., Kim, K. P., Kim, I. W., Seo, S. Y., Suh, Y. G., Kim, D. D., Shim, C. K. and Chung, S. J.: Comparison of pharmacokinetics of loxoprofen and its active metabolites after an intravenous, intramuscular, and oral administration of loxoprofen in rats: evidence for extrahepatic metabolism. *J. Pharm. Sci.*, **94**: 2187–2197 (2005).

1521-0103/345/2/271–283$25.00
THE JOURNAL OF PHARMACOLOGY AND EXPERIMENTAL THERAPEUTICS

http://dx.doi.org/10.1124/jpet.112.201814
J Pharmacol Exp Ther 345:271–283, May 2013

Long-Acting Human Serum Albumin-Thioredoxin Fusion Protein Suppresses Bleomycin-Induced Pulmonary Fibrosis Progression

Ryota Tanaka, Hiroshi Watanabe, Azusa Kodama, Victor Tuan Giam Chuang, Yu Ishima, Keisuke Hamasaki, Ken-ichiro Tanaka, Tohru Mizushima, Masaki Otagiri, and Toru Maruyama

Department of Biopharmaceutics, Graduate School of Pharmaceutical Sciences (R.T., H.W., A.K., Y.I., K.H., T.Ma.), and Center for Clinical Pharmaceutical Sciences, School of Pharmacy, Kumamoto University, Chuo-ku, Kumamoto, Japan (H.W., Y.I., T.Ma.); School of Pharmacy, Faculty of Health Sciences, Curtin Health Innovation Research Institute, Curtin University, Perth, Western Australia, Australia (V.T.G.C.); Department of Analytical Chemistry, Faculty of Pharmacy, Keio University, Minato-ku, Tokyo, Japan (K.T., T.Mi.); and Faculty of Pharmaceutical Sciences and DDS Research Institute, Sojo University, Nishi-ku, Kumamoto, Japan (M.O.)

Received November 9, 2012; accepted February 26, 2013

ABSTRACT

Idiopathic pulmonary fibrosis (IPF) is thought to involve inflammatory cells and reactive oxygen species (ROS), such as superoxide anion radical ($O_2^{\cdot-}$). There is currently no effective treatment of IPF. We previously developed a human serum albumin (HSA)–thioredoxin 1 (Trx) fusion protein (HSA-Trx) designed to overcome the unfavorable pharmacokinetic and short pharmacological properties of Trx, an antioxidative and anti-inflammatory protein. In this study, we examined the therapeutic effect of HSA-Trx on an IPF animal model of bleomycin (BLM)-induced pulmonary fibrosis. A pharmacokinetic study of HSA-Trx or Trx in BLM mice showed that the plasma retention and lung distribution of Trxc was markedly improved by fusion with HSA. A weekly intravenous administration of HSA-Trx, but not Trx, ameliorated BLM-induced fibrosis, as evidenced by a histopathological analysis and pulmonary hydroxyproline levels. HSA-Trx suppressed active-transforming growth factor (TGF)-β levels in the lung and inhibited the increase of inflammatory cells in bronchoalveolar lavage fluid, pulmonary inflammatory cytokines, and oxidative stress markers. An in vitro EPR experiment using phosphate-buffered saline–stimulated neutrophils confirmed the $O_2^{\cdot-}$ scavenging ability of HSA-Trx. Furthermore, post-treatment of HSA-Trx had a suppressive effect against BLM-induced fibrosis. These results suggest that HSA-Trx has potential as a novel therapeutic agent for IPF, because of its long-acting antioxidative and anti-inflammatory modulation effects.

Introduction

Idiopathic pulmonary fibrosis (IPF) is a chronic fibrosing interstitial pneumonia with no identifiable cause. It remains a devastating disease, with a 5-year mortality rate of 50% because of its insufficient response to medical therapy. Unfortunately, with the present lack of a complete understanding of the pathogenesis of IPF, the current treatment, which involves the use of steroids and immunosuppressants, does not improve the prognosis and recovery from the acute exacerbation of the disease (American Thoracic Society and the European Respiratory Society, 2000; Luppi et al., 2004). Therefore, the development of new drugs designed to suppress the progression of the disease or to prevent the acute exacerbation of IPF is of great importance.

Recent studies have suggested that oxidative stress plays an important role in the pathogenesis and development of IPF. In fact, increased level of reactive oxygen species (ROS), such as superoxide anion radical ($O_2^{\cdot-}$), and a decrease in the levels of glutathione and superoxide dismutase (SOD) in blood and in bronchoalveolar lavage fluid (BALF) in patients with IPF have been reported (Beeh et al., 2002; Psathakis et al., 2006). In addition, the genetic knockout of NADPH-oxidase, which increases the pulmonary level of $O_2^{\cdot-}$, resulted in the suppression of bleomycin (BLM)-induced pulmonary fibrosis in an IPF animal model. An intratracheal injection of BLM into the lungs of rodents causes alveolar cell damage, an inflammatory response, fibroblast proliferation, and subsequent collagen deposition, resembling human fibrotic lung disease (Moore and Hogaboam, 2008). In contrast, the genetic knockout of extracellular SOD, which decreases pulmonary ROS levels,

This research was supported by Japan Society for the Promotion of Science [Grant-in-Aid for Scientific Research KAKENHI 21390177]; and by Japan Science and Technology Agency, A-step feasibility study program [Grant 10801043].
dx.doi.org/10.1124/jpet.112.201814.

ABBREVIATIONS: 8-OH-dG, 8-hydroxy-2′-deoxygenase; BALF, bronchoalveolar lavage fluid; BLM, bleomycin; DMPO, 5,5-dimethyl-1-pyrroline *N*-oxide; ELISA, enzyme-linked immunosorbent assay; H&E, hematoxylin and eosin; HSA, human serum albumin; HSA-Trx, human serum albumin-thioredoxin 1 fusion protein; IL, interleukin; IPF, idiopathic pulmonary fibrosis; MDA, malondialdehyde; MIF, migration inhibitory factor; NO_2-Tyr, nitrotyrosine; OCT, optimal cutting temperature; PBS, phosphate-buffered saline; PMA, phorbol 12-myristate 13-acetate; ROS, reactive oxygen species; SOD, superoxide dismutase; TCA, trichloroacetic acid; TNF, tumor necrosis factor; Trx, thioredoxin 1.

resulted in the progression of the BLM-induced pulmonary fibrosis (Fattman et al., 2003; Manoury et al., 2005). On the other hand, the role of chronic inflammation in the pathogenesis of IPF has been the focus of a number of studies, in view of the presence of interstitial and alveolar inflammatory cells and the expression of inflammatory cytokines in the lungs of patients with IPF (Keane and Strieter, 2002). The findings of a large prospective study examining the histopathologic variability of surgical lung biopsies in 109 patients with IPF suggest an evolving disease process with chronic inflammation playing a pathogenic role (Flaherty et al., 2001). In addition, it has been well established that the levels of inflammatory cytokines and chemokines, especially interleukin (IL)-6, tumor necrosis factor (TNF)-α, and migration inhibitory factor (MIF), are markedly increased in the lungs of BLM-induced disease model animals, and it has also been reported that the knockout of IL-6 or the administration of anti-TNF-α or MIF antibodies suppress BLM-induced lung disorders (Piguet et al., 1989, 1993; Tanino et al., 2002; Chaudhary et al., 2006; Saito et al., 2008). Therefore, drugs with both antioxidative and anti-inflammatory properties would be expected to be useful in the treatment of IPF.

Thioredoxin-1 (Trx) is a small redox-active protein (M_r of ~12 kDa) that is ubiquitously present in the human body and is one of the defense proteins induced in response to various oxidative stress conditions (Holmgren, 1989; Nakamura et al., 2005). In addition to its potent antioxidative effect, which is derived from dithiol-disulfide exchange in its active site, Trx also has anti-inflammatory properties, mainly because of its ability to inhibit neutrophil chemotaxis to inflammatory sites and to suppress the expression and activation of the macrophage MIF (Nakamura et al., 2001; Tamaki et al., 2006). Because of its desirable antioxidative and anti-inflammatory properties, Trx represents a new and potentially effective therapeutic agent for the treatment of IPF. However, because Trx is eliminated extensively via glomerular filtration, its plasma half-life is only approximately 1 hour in mice and 2 hours in rats, which is extremely short in terms of producing a significant therapeutic impact (Nakamura et al., 2001; Ueda et al., 2006). To obtain a satisfactory therapeutic outcome, a sustainable therapeutic concentration of Trx would be needed. To achieve this, constant infusion or frequent repeated administrations of Trx would be required (Hoshino et al., 2003; Liu et al., 2004; Ueda et al., 2006). Hoshino et al. (2003) demonstrated that exogenous recombinant Trx was effective in inhibiting BLM-induced lung damage when administered intraperitoneally or via a continuous infusion of Trx that is repeated at 2-day intervals.

In an attempt to increase the blood retention time of Trx, we recently produced a genetically engineered fusion protein of human serum albumin (HSA) and Trx (HSA-Trx) with use of a *Pichia* expression system. The plasma half-life of the HSA-Trx fusion protein in normal mice was found to be similar to that of HSA, which is 10 times longer than the plasma half-life of Trx (Ikuta et al., 2010). Of interest, HSA-Trx showed a higher distribution to the lungs than did Trx. Therefore, a further attempt will be made to investigate the clinical usefulness of HSA-Trx in treating oxidative stress and inflammation-related lung disorders.

The purpose of this study was to investigate the therapeutic impact of HSA-Trx in the treatment of IPF. With use of the BLM-induced pulmonary fibrosis animal model, the results showed that HSA-Trx could prevent BLM-induced pulmonary fibrosis through its long-acting antioxidative and anti-inflammatory modulation effects.

Materials and Methods

BLM was purchased from Nippon Kayaku (Tokyo, Japan). Mayer's hematoxylin, a 1% eosin alcohol solution, mounting medium for histologic examinations (malinol), and Masson's trichrome staining reagents were from Muto Pure Chemicals (Tokyo, Japan). Optimal cutting temperature (OCT) compound was purchased from Sakura Finetek (Tokyo, Japan). Chloral hydrate, chloramine T, and phorbol 12-myristate 13-acetate (PMA) were obtained from Sigma-Aldrich (Tokyo, Japan). Paraformaldehyde, trichloroacetic acid (TCA), perchloric acid, and 4-(dimethylamino)-benzaldehyde were from Nacalai Tesque (Kyoto, Japan). Diethylene-triamine-pentaacetic acid was purchased from Dojindo Laboratories (Kumamoto, Japan); 5,5-dimethyl-1-pyrroline *N*-oxide (DMPO) was purchased from Alexis Biochemicals (Lausen, Switzerland). The TGF-β1 enzyme-linked immunosorbent assay (ELISA) kit was purchased from R&D Systems Inc. (Minneapolis, MN). IL-6 and TNF-α ELISA kit were purchased from Biolegend (San Diego, CA). Sea-ICR mice (age, 6 weeks; male) were obtained from Kyudo Co., Ltd. (Saga, Japan). Other chemicals used were obtained from commercial suppliers.

Production of HSA-Trx Fusion Protein. Trx and HSA fusion protein was produced in accordance with the method reported previously (Ikuta et al., 2010; Furukawa et al., 2011) with a slight modification. The transformed *Pichia pastoris* was incubated in 1.25 liters of growth phase media, BMGY (1% yeast extract, 2% peptone, 100 mM potassium phosphate [pH 6.0], 1.34% yeast nitrogen base with ammonium sulfate without amino acids, 4×10^{-5} % biotin, 1% glycerol) for 2 days (OD_{600} = 2). It was then cultured in 800 ml of protein induction phase media, BMMY (1% yeast extract, 2% peptone, 100 mM potassium phosphate [pH 6.0], 1.34% yeast nitrogen base with ammonium sulfate without amino acids, 4×10^{-5} % biotin, 1% methanol) for 3 days at 30°C. Methanol was added every 24 hours so that the concentration of methanol was maintained at 1% to sustain the protein expression induction effect. The secreted fusion protein was isolated from the growth media as follows. The solution was loaded on to a column of Blue Sepharose 6 Fast Flow column (GE Healthcare, Tokyo, Japan) equilibrated with 200 mM sodium acetate buffer (pH 5.5) after the medium was dialyzed against the same buffer. The column was washed with ~5 bed volumes of 200 mM sodium acetate buffer (pH 5.5), and then the fusion protein was eluted with 20 mM sodium acetate buffer (pH 6.5) containing 3 M NaCl. Next, with use of AKTA prime, the eluate was loaded onto a column of 5-ml HiTrap Phenyl HP column (GE Healthcare) for hydrophobic chromatography with the following conditions (buffer A, 0 mM Tris-HCl/1.5 M ammonium sulfate [pH 7.0]; buffer B, 50 mM Tris-HCl [pH 7.0]; gradient, 0–100% [buffer B] 100 ml; flow rate, 3 ml/min). The desired fusion protein was obtained by delipidation with activated carbon treatment, as described by Chen (1967). The fusion protein was analyzed using SDS-PAGE and native SDS-PAGE using a 15% polyacrylamide gel, with Coomassie Blue R250 staining. The purity of the fusion protein was estimated to be more than 95% (Ikuta et al., 2010).

Production of BLM-Induced Pulmonary Fibrosis Mice Model. All animal experiments were conducted in accordance with the guidelines of Kumamoto University for the care and use of laboratory animals. BLM-induced pulmonary fibrosis model mice were produced by intratracheal injection of BLM (5 mg/kg) in phosphate-buffered saline (PBS; 1 ml/kg) under anesthesia with chloral hydrate (500 mg/kg) on day 0 (Tanaka et al., 2010). Either Trx or HSA-Trx was administered (but not both) intravenously (3.5 nmol protein in 200 μl PBS/mouse) via the mouse tail vein 30 minutes before BLM treatment (day 0). HSA-Trx was administered intravenously on days 0 and 7 (refer to every 1 week, Fig. 1A) or only on day 0 (refer to every 2 weeks, Fig. 1A). For an intervention study, the first dose of HSA-Trx was administered 1 day after the BLM treatment, and the subsequent dose was administered on day 7 after the BLM treatment. (Fig. 1C).

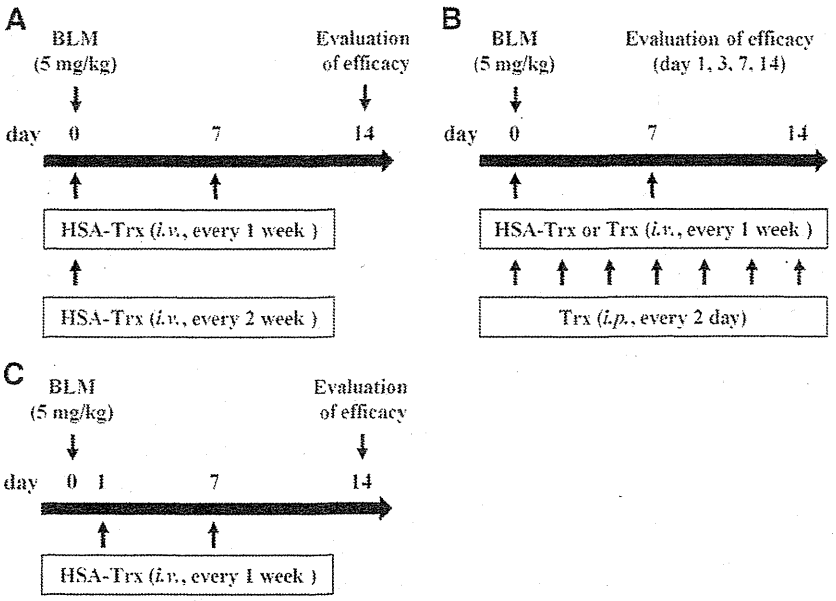

Fig. 1. Schematic summary of the experimental protocol for evaluating the effect of HSA-Trx on BLM-induced pulmonary fibrosis used in the study. HSA-Trx was administrated intravenously on days 0 and 7 (every 1 week; A) or only on day 0 (every 2 weeks; A). On day 0, HSA-Trx was administered 30 minutes before BLM treatment. For the intervention study, the first dose of HSA-Trx was administered 1 day after BLM treatment, and the subsequent dose was administered at day 7 after BLM treatment (C).

Histopathological Analysis of Lung Tissue (Hematoxylin and Eosin Staining and Masson's Trichrome Staining of Collagen). On day 14 after BLM administration, the whole lungs were flushed with 4% paraformaldehyde before being removed. The removed lungs were fixed in 4% buffered paraformaldehyde and then embedded in paraffin before being cut into 4-μm-thick sections. For hematoxylin and eosin (H&E) staining, sections were stained first with Mayer's hematoxylin and then with 1% eosin alcohol solution. For Masson's trichrome staining, sections were sequentially treated with solution A [5% (wt/vol) potassium dichromate and 5% (wt/vol) TCA], Weigert's iron hematoxylin, solution B [1.25% (wt/vol) phosphotungstic acid and 1.25% (wt/vol) phosophomolybdic acid], 0.75% (wt/vol) Orange G solution, solution C [0.12% (wt/vol) xylidine Ponceau, 0.04% (wt/vol) acid fuchsin, and 0.02% (wt/vol) azophloxin], 2.5% (wt/vol) phosphotungstic acid, and finally an aniline blue solution. H&E and Masson's trichrome staining samples were mounted with malinol and inspected using a microscope (BZ-8000; Keyence, Osaka, Japan).

Determination of Lung Fibrosis. Fibrosis score was evaluated (×100) as the quantity of the section positively stained for collagen and displaying alveolar wall thickening (1 = <25%, 2 = 25–50%, 3 = 50–75%, and 4 = 75–100%) (Gibbons et al., 2011). Only fields in which most of the field was composed of alveoli were scored. The entire lung section was analyzed. The investigator was masked to each sample.

Determination of Hydroxyproline Level in Lung Tissues. Hydroxyproline content was determined as described previously (Woessner, 1961). On day 14 after BLM administration, the right lung was removed and homogenized in 1 ml of 5% TCA. After centrifugation, the pellets were hydrolyzed in 0.5 ml of 10 N HCl for 16 hours at 110°C. Each sample was incubated for 20 minutes at room temperature after the addition of 0.5 ml of 1.4% (wt/vol) chloramine T solution and then incubated at 65°C for 10 minutes after addition of 0.5 ml of Ehrlich's reagent (1 M DMBA, 70% [vol/vol] isopropanol and 30% [vol/vol] perchloric acid). The absorbance was measured at 550 nm to determine the amount of hydroxyproline.

Quantification of Activated TGF-β1, IL-6, and TNF-α and Western Blot Analysis of Macrophage MIF in Lung Tissue. On days 3 and 7 after BLM administration, the whole lungs were removed and homogenized in 0.5 ml of buffer (PBS, 1% protease inhibitor cocktail, 10 mM EDTA, 0.05% Tween 20). After centrifugation at 21,000*g* for 10 minutes at 4°C (two times), the supernatants were recovered. The amounts of active TGF-β1 (day 7), IL-6, and TNF-α (days 3 and 7) in the supernatant were measured using ELISA, according to the manufacturer's protocol. In addition, Western blotting of MIF chemokine in the supernatant was performed using the following protocol. After measurement of the protein content with use of the BCA protein assay reagent (Pierce Biotechnology Inc., Rockford, IL), each sample was separated by 12.5% SDS-PAGE and transferred onto polyvinylidene difluoride membranes (Immobilon-P; Millipore, Bedford, MA) by wet electroblotting. The membranes were blocked for 1 hour at room temperature with 5% skim milk in PBS. The membranes were washed three times with PBS containing 0.05% Tween 20 (PBS-T) and incubated for 2 hours at room temperature with a 400 ng/ml primary mouse monoclonal antibody against N terminus of MIF of human origin, which has cross-reactivity with mouse MIF (sc-271631; Santa Cruz Biotechnology Inc., Santa Cruz, CA) in PBS-T. The membranes were washed 3 times with PBS-T and incubated with the secondary antibody (horseradish peroxidase-linked anti-mouse IgG [H+L]; Invitrogen, Carlsbad, CA) for 1.5 hours at room temperature. The membranes were washed 3 times with PBS-T, and immunoblots were visualized using the SuperSignal West Pico chemiluminescent substrate (Pierce Biotechnology Inc.) with LAS-4000EPUVmini (Fujifilm, Tokyo, Japan).

Counting of Cells in BALF. On days 1 and 3 after BLM administration, the mice were anesthetized with pentobarbital, the chests were opened, and blood was drained. BALF samples were collected by cannulating the trachea and lavaging the lung with 1 ml of sterile PBS containing 50 U/ml heparin (two times). Approximately 1.8 ml of BALF was routinely recovered from each animal. The BALF was centrifuged at 4100*g* for 5 minutes at 4°C to separate the cells in the BALF from the liquid. Cells were dissolved in 0.9% NaCl, and lysate was centrifuged again. From the recovered cells, the total cell number was counted using a hemocytometer. Cells were stained with Diff-Quick reagents (Kokusai Shiyaku, Kobe, Japan), and the ratios of alveolar macrophages, neutrophils, and lymphocytes to total cells were determined. More than 200 cells were counted for each sample.

Immunostaining of Lungs Tissue. On day 3 after BLM administration, the whole lungs were flushed with sterile PBS before being removed. The removed lungs were stored in 4% paraformaldehyde at 4°C for 2 hours before being immersed in a 10% sucrose solution overnight. The concentration of sucrose solution was then adjusted to 20% at room temperature, and incubation was continued for another 6 hours. The recovered lungs were covered with OCT compound and frozen at −80°C. Next, the lungs frozen with cryostat (CM3000II; Leica, Wetzlar, Germany) were sliced at a thickness of 4 μm and attached on a glass slide. The slide was then cleansed to remove OCT compound and dried. After drying the slide completely,

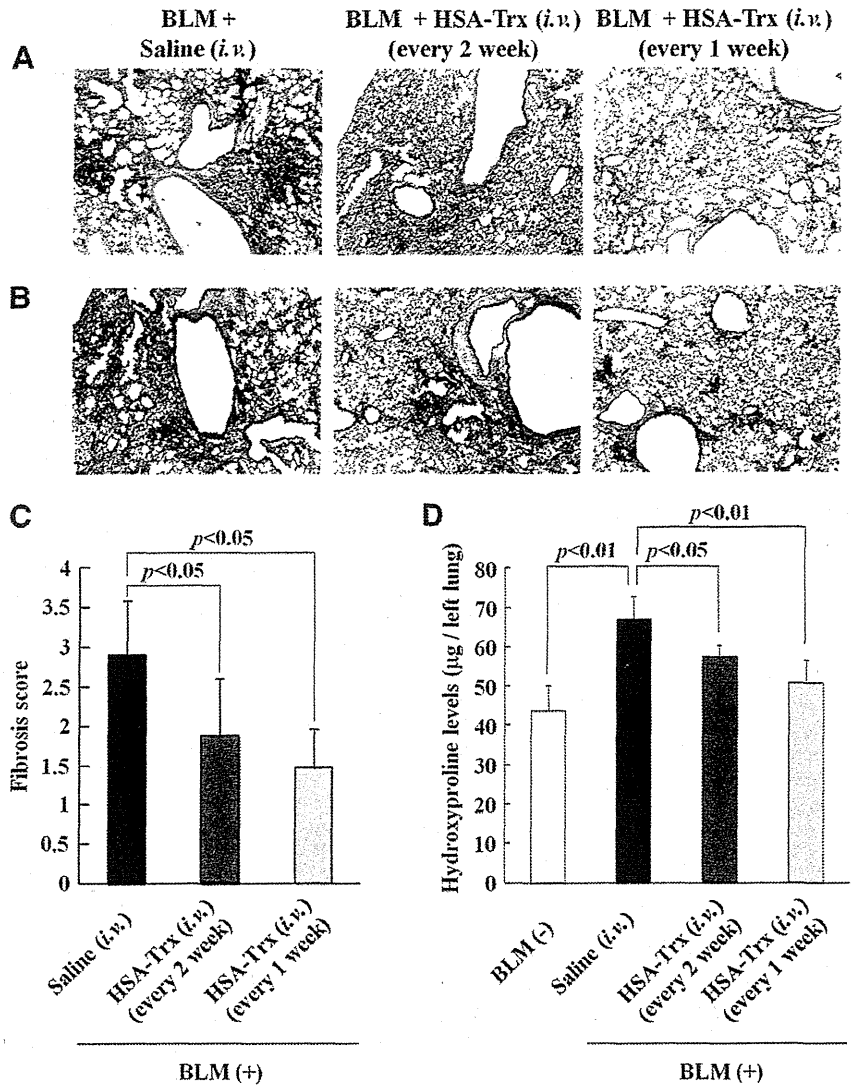

Fig. 2. Effect of HSA-Trx (intravenously; every 2 weeks or every 1 week) on the BLM-induced pulmonary fibrosis. (A and B) Sections of pulmonary tissue were prepared 14 days after BLM administration and subjected to histopathological examination [H&E (A) and Masson's trichrome staining (B)]. (C) Fibrosis score was evaluated as the quantity of the section positively stained for collagen and displaying alveolar wall thickening. (D) Hydroxyproline levels in lung were determined 14 day after BLM administration. Each bar represents the mean ± S.D. (C, n = 3–5; D, n = 5).

a solution containing 50 mM Tris/HCl + 0.1% Tween 20 (T-TB) was used to solubilize the lung slice, followed by blocking with Block Ace (Dainippon Pharmaceutics, Osaka, Japan) at room temperature for 15 minutes. Next, the primary antibody reaction was conducted below 4°C overnight. In addition, the primary mouse monoclonal antibody against 8-hydroxy-2′-deoxygenase (8-OH-dG) [15A3] (sc-66036; Santa Cruz Biotechnology Inc.), which has cross-reactivity with mouse, or the primary rabbit polyclonal antibody against nitrotyrosine (NO_2-Tyr;AB5411; Millipore, Billerica, MA), which has cross-reactivity with mouse, was diluted to 2 or 20 μg/ml before use, respectively. The lung slices were then washed with 50 mM Tris/HCl (TB) and T-TB, followed by the secondary antibody reaction at room temperature for 1.5 hours. For the secondary antibody, in relation to NO_2-Tyr and 8-OH-dG, Alexa Fluor 546 goat anti-mouse IgG (H+L; Invitrogen) and Alexa Fluor 488 goat anti-mouse IgG (H+L; Invitrogen) diluted 200 times were respectively used. After the reaction, the slide was observed using a microscope (BZ-8000; Keyence). Image analyses of the extent and intensity of 8-OH-dG and NO_2-Tyr staining were also performed using ImageJ software.

Determination of Malondialdehyde in Lung Tissue. On day 3 after BLM administration, the right lung was removed and homogenized in 0.5 ml of radioimmunoprecipitation assay/PI buffer (150 mM NaCl, 1% Nonidet P-40, 10 mM Tris-HCl, pH 7.4, including a 1% solution of a protease inhibitor; Nacalai Tesque, Tokyo, Japan). After centrifugation, the amount of malondialdehyde (MDA) in supernatant was measured using thiobarbituric acid reactive substances assay kit (Cayman Chemical, Ann Arbor, MI), which is a well-established method for measuring lipid peroxidation, according to the manufacturer's protocol.

Isolation of Polymorphonuclear Neutrophils. Whole blood was obtained from 10 mice. Heparinized blood was mixed with an equal volume of 3% dextran in 0.9% NaCl. After 30 minutes of gravity sedimentation, the upper layer, containing leukocytes, was removed and centrifuged at 620g for 10 minutes. The cell pellet was resuspended in 0.9% NaCl and underlaid with Ficoll-Paque (GE Healthcare). After centrifugation for 30 minutes at 1490g, the mononuclear cell layer was isolated, and contaminating red blood cells were removed by hypotonic lysis. After centrifugation for 10 minutes at 760g (two times), the pellet was resuspended, and the neutrophils were plated at 1.0×10^6 cells/ml in PBS.

Measurement of Neutrophil-Derived ROS. The scavenging activity of HSA-Trx against $O_2^{\cdot-}$ released from neutrophils was determined using EPR spin trapping with DMPO. The neutrophils (1.0×10^6 cells/ml) were pretreated with PMA (1 μg/ml) for 7 minutes at 37°C to activate the cells and generate ROS. Aliquots of this cell suspension were combined with 100 μM DTPA in Hanks' balanced salt solution in the absence or presence of either HSA-Trx (10, 30, 50 μM), HSA (30 μM), or Trx (30 μM). After activation of neutrophils,